Spectroscopic study of the dehydration and/or dehydroxylation of phyllosilicate and zeolite minerals

Congcong Che,[1] Timothy D. Glotch,[1] David L. Bish,[2] Joseph R. Michalski,[3] and Wenqian Xu[1]

Received 6 September 2010; revised 12 February 2011; accepted 1 March 2011; published 25 May 2011.

[1] Phyllosilicates on Mars mapped by infrared spectroscopic techniques could have been affected by dehydration and/or dehydroxylation associated with chemical weathering in hyperarid conditions, volcanism or shock heating associated with meteor impact. The effects of heat-induced dehydration and/or dehydroxylation on the infrared spectra of 14 phyllosilicates from four structural groups (kaolinite, smectite, sepiolite-palygorskite, and chlorite) and two natural zeolites are reported here. Pressed powders of size-separated phyllosilicate and natural zeolite samples were heated incrementally from 100°C to 900°C, cooled to room temperature, and measured using multiple spectroscopic techniques: midinfrared (400–4000 cm^{-1}) attenuated total reflectance, midinfrared reflectance (400–1400 cm^{-1}), and far-infrared reflectance (50–600 cm^{-1}) spectroscopies. Correlated thermogravimetric analysis and X-ray diffraction data were also acquired in order to clarify the thermal transformation of each sample. For phyllosilicate samples, the OH stretching (~3600 cm^{-1}), OH bending (~590–950 cm^{-1}), and/or H_2O bending (~1630 cm^{-1}) bands all become very weak or completely disappear upon heating to temperatures > 500°C. The spectral changes associated with SiO_4 vibrations (~1000 cm^{-1} and ~500 cm^{-1}) show large variations depending on the compositions and structures of phyllosilicates. The thermal behavior of phyllosilicate IR spectra is also affected by the type of octahedral cations. For example, spectral features of Al^{3+}-rich smectites are more stable than those of Fe^{3+}-rich smectites. The high-temperature (>800°C) spectral changes of trioctahedral Mg^{2+}-rich phyllosilicates such as hectorite, saponite, and sepiolite result primarily from crystallization of enstatite. Phyllosilicates with moderate Mg^{2+} concentration (e.g., palygorskite, clinochlore) and dioctahedral montmorillonites (e.g., SAz-1 and SCa-3) with partial Mg^{2+}-for-Al^{3+} substitution all have new spectral feature developed at ~900 cm^{-1} upon heating to 800°C. Compared with phyllosilicates, spectral features of two natural zeolites, clinoptilolite and mordenite, are less affected by thermal treatments. Even after heating to 900°C, the IR spectral features attributed to Si (Al)-O stretching and bending vibration modes do not show significant differences from those of unheated zeolites.

Citation: Che, C., T. D. Glotch, D. L. Bish, J. R. Michalski, and W. Xu (2011), Spectroscopic study of the dehydration and/or dehydroxylation of phyllosilicate and zeolite minerals, *J. Geophys. Res.*, *116*, E05007, doi:10.1029/2010JE003740.

1. Introduction

[2] Data from the Mars Express Observatoire pour la Minéralogie, l'Eau, les Glaces, et l'Activité (MEx/OMEGA) and Compact Reconnassaince Imaging Spectrometer for Mars (MRO/CRISM) visible and near infrared imaging spectrometers have shown phyllosilicates to be present on the Martian surface [*Poulet et al.*, 2005; *Bibring et al.*, 2006; *Loizeau et al.*, 2007; *Mangold et al.*, 2007]. The identification of phyllosilicates is based on the detection of ~1.4 μm (the first overtone of the O-H stretching modes), ~1.9 μm (H-O-H band) and ~2.15–2.4 μm (metal-OH bands) features. Phyllosilicates are detected in a number of contexts on Mars, primarily associated with ancient, layered terrain, deep clay deposits exposed in canyon walls or exhumed by impact craters, or remobilized units in the highlands corresponding to intracrater fans and deltas [*Poulet et al.*, 2005; *Bibring et al.*, 2006; *Poulet et al.*, 2007; *Mustard et al.*, 2008; *Murchie et al.*, 2009].

[3] However, analysis of mid-IR region (5–50 μm) covered by Thermal Emission Spectrometer (TES) has not unambiguously detected phyllosilicates on the surface of Mars. The TES Surface Type 2 (ST2) was initially interpreted as a basaltic andesite [*Bandfield et al.*, 2000]. Later, *Wyatt and McSween* [2002] showed that weathered basaltic composition including clays could also produce an acceptable model

[1]Department of Geosciences, State University of New York at Stony Brook, Stony Brook, New York, USA.
[2]Department of Geological Sciences, Indiana University, Bloomington, Indiana, USA.
[3]Planetary Science Institute,Tucson, Arizona, USA.

0148-0227/11/2010JE003740

fit. Still there is no definitive evidence in TES data showing that clay minerals dominate any particular geographic region of Mars or are globally distributed because it is difficult to distinguish phyllosilicates from other high silica phases in TES data at global scale [*Bandfield*, 2002; *Ruff*, 2003; *Michalski et al.*, 2005, 2006; *Ruff and Christensen*, 2007]. Recent studies show it can be possible to identify phyllosilicates at local scales: thermal emission spectra can be used to delineate phyllosilicate deposits from their long-wavelength spectra features [*Ruff and Christensen*, 2007; *Michalski et al.*, 2010]. However, in general TES spectra of the same deposits where OMEGA and CRISM delineate phyllosilicate occurrences do not show unambiguous evidence for these minerals. One reason for this disconnect could be that Martian phyllosilicates could have structures modified by postdepositional processes which would affect near infrared and thermal infrared spectral properties in different ways.

[4] Phyllosilicates detected on the surface of Mars have been primarily dated as early-to-mid Noachian in age [*Bibring et al.*, 2005; *Poulet et al.*, 2005; *Mustard et al.*, 2007], which suggests phyllosilicates on Mars may have been altered by multiple processes (e.g., chemical weathering in hyperarid conditions, volcanism or shock heating associated with meteor impact). Impact events may be one of the most important processes that affected phyllosilicates. It is possible that the phyllosilicates were repeatedly subjected to high temperatures resulting from impact processes and continuous exposure to high temperatures is likely to lead to the dehydration and/or dehydroxylation of phyllosilicates. Both their structural properties and spectral features could have been modified significantly by high temperature and pressure induced by impact shocking. Previous studies showed suggestive evidence of dehydrated and/or dehydroxylated phyllosilicates on Mars.

[5] Mawrth Vallis has been studied by several authors because this region is potentially significant for understanding the different climatic and geologic environments of ancient Mars [*Poulet et al.*, 2005; *Michalski and Noe Dobrea*, 2007; *Loizeau et al.*, 2007; *Bishop et al.*, 2008a, 2009; *Farrand et al.*, 2009; *Michalski and Fergason*, 2009]. The distribution of phyllosilicates detected near Mawrth Vallis corresponds to the light-toned deposits in the surrounding Noachian plains [*Loizeau et al.*, 2007]. However, *Loizeau et al.* [2007] noticed a lack of phyllosilicates on a few bright outcrops near Mawrth Vallis. For example, they did not find any evidence showing the presence of phyllosilicates on a bright outcrop which was located on the west of Mawrth Vallis. Processes of dehydration and/or dehydroxylation were among the reasons they hypothesized to explain this observation. *Michalski and Noe Dobrea* [2007] also pointed out that all the phyllosilicates identified near Mawrth Vallis are associated with light-tone bedrock, but not all light-toned bedrock contains phyllosilicates. *Milliken et al.* [2007] calculated and produced a hydration map for Mawrth Vallis region by examining the strength of the ~3 μm absorption of OMEGA data. The estimated water content of the bright outcrop without phyllosilicate detection as described by *Loizeau et al.*'s [2007] work is significantly less than that of the bright outcrops mantled by phyllosilicates, but still higher than surrounding terrains with similar albedo values. This result is consistent with the possibility that the outcrop on the west of Mawrth Vallis is covered by dehydrated and/or dehydroxylated phyllosilicates.

[6] A recent study by *Gavin and Chevrier* [2010] showed that near-infrared spectral features from the ejecta of Toro crater are more consistent with those of thermally treated nontronite. *Fairén et al.* [2010] calculated the maximum temperature increases in a transient crater and their model showed that temperatures can reach as high as 1000°C in certain areas. Not only do meteoric impacts induce flash heating of the target, but they also deposit a significant amount of energy into the planetary surface that could lead to longer term heating of the target rocks. In the impact-induced hydrothermal systems modeled by *Abramov and Kring* [2005], they calculated that temperature as high as 1200°C can last for tens of thousands of years. In the laboratory, temperatures as low as 500–700°C are sufficient to cause the complete dehydration and/or dehydroxylation of most phyllosilicates within 24 h [e.g., *Guggenheim and Koster van Groos*, 2001]. Examinations of meteorites by several authors suggested that shock heating plays a major role in the modification of phyllosilicates [*Ohnishi and Tomeoka*, 2002; *Tonui et al.*, 2003; *Tomioka et al.*, 2007]. Relatively little work has been done to systematically analyze the effects of shock on phyllosilicates, though previous authors demonstrated that phyllosilicates (serpentine, nontronite) do in fact lose volatiles due to shock pressures and shock heating [*Boslough et al.*, 1980; *Lange and Ahrens*, 1982]. In addition, serpentines that have not lost their OH during shock appear to be more susceptible to dehydroxylation postshock than their unshocked counterparts, as a result of increased disorder in their structures [*Tyburczy and Ahrens*, 1988]. Recent work on near infrared (NIR) spectroscopy of a shocked sample of nontronite revealed few spectral changes as a function of impactor velocity [*Gavin et al.*, 2008], but this work did not provide details on the interpreted shock pressures or the amount of volatile loss. All of the previous work shows, however, that volatile loss in phyllosilicates occurs as a result of shock pressure. The combined effects of shock heating and shock pressure are difficult to analyze together in the laboratory. However, these effects can be analyzed independently, and the effects of heat-induced dehydration and/or dehydroxylation are analyzed here.

[7] The objective of this study is to characterize the mid-to-far-IR spectral features of phyllosilicates from four groups (smectite, kaolinite, chlorite, and sepiolite-palygorskite) that have been heated to increasingly higher temperatures in order to gain insights into the crystal structures of phyllosilicates at different temperatures and to enable future identification of these types of minerals on Mars. A subsequent paper will examine the effect of dehydration and/or dehydroxylation on visible and near IR (VNIR) reflectance spectra.

[8] In addition to phyllosilicates, we also analyzed the spectral features of two natural zeolite minerals as a part of this study. Zeolites may be another important class of minerals that are present on the surface of Mars in a hydrated state [*Bish et al.*, 2003]. *Ruff* [2004] has provided some evidence of zeolites in Martian surface dust using TES data and using CRISM near-infrared spectral data, *Ehlmann et al.* [2009] identified zeolites in craters west of Nili Fossae. Zeolites have chemical compositions similar to phyllosilicates and they are common hydrous alteration products of

basaltic rocks. Therefore study of both phyllosilicates and zeolites can provide a more comprehensive spectral feature library for dehydrated and/or dehydroxylated aluminosilicate minerals.

2. Background

2.1. Brief Review of Phyllosilicate and Zeolite Structures

[9] The crystal structures of phyllosilicate minerals are well known and only basic information will be provided here in order to provide context for the spectroscopy results [*Farmer*, 1974; *Bailey*, 1980; *Moore and Reynolds*, 1989a].

[10] There are many kinds of phyllosilicates due to the possible structural and chemical variations within this mineral family, but most have the typical layer structures composed of two different kinds of sheets: tetrahedral sheets (T) and octahedral sheets. The dominant cation (normally Si^{4+}, Al^{3+}, or Fe^{3+}) in the tetrahedral sheet(s) is tetrahedrally coordinated to four oxygen anions and the corner-linked tetrahedra extend infinitely in two dimensions. Individual tetrahedral sheets have a composition of T_2O_5, but the Si/O ratio varies from 0.3 to 0.4 as Si^{4+} cations are replaced by Al^{3+} or Fe^{3+} to various extents. The octahedral sheet can be described as a sheet of edge-linked octahedra, extending infinitely in the same two dimensions as the tetrahedral sheets. The octahedral cations are typically Al^{3+}, Mg^{2+}, Fe^{3+}, or Fe^{2+}, but most other transition elements (except Sc) and Li can occur in some minerals. Cations in the octahedral sheet are octahedrally coordinated to oxygens and hydroxyls. The tetrahedral sheets and octahedral sheet are linked together by shared apical oxygens to form the layer structures. Unlike the tetrahedra, not all of octahedral sites must be filled by cations. The smallest structural unit contains three octahedra and the number of cations can vary between two and three, to meet the general requirement of a total positive charge of six for these three sites. For example, there could be 3 Mg^{2+} ions or 2 Al^{3+} ions in the octahedral sites. When three ions are present, the structure is called trioctahedral, and if only two of the three sites are occupied, it is called dioctahedral.

[11] Phyllosilicates selected for this study can be divided into four groups according to their structural type: the kaolinite-serpentine group, smectite group, chlorite group, and sepiolite-palygorskite group. The kaolinite-serpentine group minerals are characterized by uncharged 1:1 (one octahedral sheet is linked to one tetrahedral sheet) layers, and they contain no cations or H_2O molecules in their interlayers. Minerals of the smectite group are all 2:1 (one octahedral sheet is linked to two tetrahedral sheets, one on each side) layers and they have interlayer cations to balance a negative charge on the 2:1 layers. They also typically contain H_2O molecules in their interlayer region. Both dioctahedral and trioctahedral smectite minerals are discussed here. Members of the chlorite group also have a negatively charged 2:1 layer structure, but they have positively charged $(R^{2+}, R^{3+})_3(OH)_6$ octahedral sheets in the interlayers instead of large cations and H_2O molecules. Sepiolite and palygorskite (also known as attapulgite) also contain 2:1 layers in their structural units but they are different from other phyllosilicates. Sepiolite and palygorskite have similar ribbon-like morphologies and their octahedral and tetrahedral sheets are divided into ribbons by inversion, although the tetrahedral sheets are still linked. The alternating channels between ribbon strips are occupied by H_2O molecules and exchangeable cations.

[12] Zeolites are microporous aluminosilicates and their structures have been summarized by *Breck* [1974a], *Barrer* [1978, 1982], *Newsam* [1986], and *Armbruster and Gunter* [2001]. Zeolites are composed of $(SiO_4)^{4-}$ and $(AlO_4)^{5-}$ tetrahedra that share oxygen atoms, and they have chemical compositions similar to phyllosilicates. However, compared with phyllosilicates characterized by layer structures, zeolites have a three-dimensionally linked crystal structure. The $(SiO_4)^{4-}$ and $(AlO_4)^{5-}$ tetrahedra are linked together to form a framework consisting of interconnected tunnels and cages. Ions of suitable size such as K^+, Ca^{2+}, and Na^+ can enter into the extraframework sites in zeolites, and H_2O molecules can also exist inside the porous structures.

2.2. Previous Studies of Dehydration and/or Dehydroxylation of Phyllosilicates and Zeolites

[13] Many techniques have been used to analyze the dehydration and/or dehydroxylation behaviors of phyllosilicates in the past. Infrared (IR) spectroscopy, thermogravimetric analysis (TGA), X-ray diffraction (XRD) analysis, and nuclear magnetic resonance (NMR) spectroscopy are the most important of them.

[14] TGA is the most direct tool to observe the temperature dependence of mineral mass. XRD is the most common technique used to study changes in crystal structure when a mineral is heated or exposed to different atmospheres [e.g., *Harris et al.*, 1992; *Aceman et al.*, 1997; *Sarikaya et al.*, 2000], and NMR spectroscopy can help to follow the changes in the coordination environments of H, Si, Al, and interlayer cations within phyllosilicates and zeolites caused by thermal treatment [e.g., *Frost and Barron*, 1984; *Fitzgerald et al.*, 1989, 1996; *Sanchez-Soto et al.*, 1993; *Carroll et al.*, 2005; *Roch et al.*, 1998; *Drachman et al.*, 1997; *Sanz et al.*, 1988; *Lambert et al.*, 1989; *Rocha and Klinowski*, 1990; *Slade and Davies*, 1991; *Massiot et al.*, 1995; *Rocha*, 1999; *McManus et al.*, 2001; *He et al.*, 2003]. Of these, TGA and XRD analysis were utilized in this study to complement IR spectroscopy, and NMR will be used in the extension of this present work.

[15] *Grim and Kulbicki* [1961] published IR transmission spectra of about forty montmorillonite-group samples after heating to 1400°C. *Bruckenthal and Singer* [1987] suggested that dehydrated phyllosilicates may exist on Mars and several asteroids due to the anhydrous nature of the extraterrestrial environment. They reported the NIR reflectance (~0.5–4.5 μm) spectra of hydrated 1:1 and 2:1 layer phyllosilicates (including serpentine, talc, Ca-montmorillonite, and saponite) and their heating products (120, 160, 200, 250, 300, 400, 600, and 750°C), in order to provide information for future spectroscopic observations of other planets. *Villieras et al.* [1994] used transmission infrared spectroscopy (400–4000 cm^{-1}) to study the thermal modifications of chlorite. Further infrared spectroscopic studies of dehydrated and/or dehydroxylated phyllosilicates developed gradually over the past 10 years. *Kloprogge et al.* [1999a, 1999b, 2000] and *Kloprogge and Frost* [2005] published a series of reports about emission (400–4000 cm^{-1}) analysis of dehydroxylated phyllosilicates including smectite group, kaolinite group,

Table 1. Summary of Phyllosilicates and Zeolites for This Study

Structural Group	Mineral	Sample Number	Source	Size Fraction
Kaolinite-serpentine group	kaolinite	KGa-1b	CMS	<2 μm
Smectite group	montmorillonite ("Cheto")	SAz-1	CMS	<2 μm
	montmorillonite ("Otay")	SCa-3	CMS	<2 μm
	Ca-montmorillonite	STx-1	CMS	<2 μm
	Na-montmorillonite	SWy-2	CMS	<2 μm
	saponite	SapCa-2	CMS	<2 μm
	beidellite	SBCa-1	CMS	<2 μm
	mica-montmorillonite	Syn-1	CMS	<2 μm
	hectorite	SHCa-1	CMS	<2 μm
	nontronite	NAu-1	CMS	<2 μm
	nontronite	NAu-2	CMS	<2 μm
Chlorite group	clinochlore	clinochlore	mineral unlimited	<2 μm
Sepiolite-palygorskite group	palygorskite (attapulgite)	PFl-1	CMS	<2 μm
	sepiolite	SepSp-1	CMS	<2 μm
Zeolite group	mordenite	27133	mineral research	<2 μm
	clinoptilolite	27031	mineral research	<2 μm

and chlorite group minerals. However, their technique was considered a transmission measurement according to the different definitions of radiance and emissivity [*Michalski et al.*, 2006]. *Milliken and Mustard* [2005] acquired reflectance spectra (1.3–5.0 μm) of five hydrated materials (including montmorillonite and clinoptilolite) at different temperatures in order to quantify the H_2O content of hydrated minerals. *Gavin and Chevrier* [2010] thermally treated nontronite and montmorillonite and used NIR (1.0–2.5 μm) reflectance spectra to characterize the structural changes occurring on heating. They showed that high-temperature (above 1000°C) heating causes all NIR spectral features to disappear.

[16] Most studies of the dehydration of natural zeolites have been based on thermogravimetric analysis (TGA), differential thermal analysis (DTA), and XRD measurements. The extraframework cation compositions [*Bish*, 1988], the energetics of the H_2O in the zeolite channels [*Bish and Carey*, 2001], the Si/Al ratio of a zeolite, and the ionic potential [*Cruciani*, 2006] all affect the thermal behavior of natural zeolites significantly. Relatively fewer results have been reported on the infrared spectroscopy of dehydrated natural zeolites. *Rodriguez-Fuentes et al.*'s [1998] work suggested that the IR spectral features (400–1700 cm^{-1}) of clinoptilolite and heulandite samples were most affected by their exchangeable cation composition and the history of thermal treatment. The dehydration processes of naturally occurring zeolites (including stilbite and mesolite) were investigated by in situ FTIR spectroscopy (400–8000 cm^{-1}) by *Prasad et al.* [2005] and *Prasad and Prasad* [2007], who reported the IR absorbance spectra of dehydrated natural zeolites.

2.3. The Significance of This Work

[17] Although the dehydration and/or dehydroxylation behaviors of phyllosilicates and zeolites have been studied extensively in the past, there is no substantive work thoroughly describing the mid-to-far-IR spectral reflectance changes of these minerals upon heating. In section 1, we hypothesized that dehydrated and/or dehydroxylated phyllosilicates due to impact heating may remain on Mars. NIR spectra cannot identify these possible dehydrated and/or dehydroxylated phases because phyllosilicates show almost no spectral feature in near-IR region after they have been heated to high temperatures [*Milliken and Mustard*, 2005; *Gavin and Chevrier*, 2010; *Che and Glotch*, 2010]. Therefore it is very important to understand the effects of temperature on the mid-IR spectra of phyllosilicates.

[18] In this study, we (1) report how the mid-IR attenuated total reflectance (ATR) and mid-to-far-IR specular reflectance spectra of phyllosilicates and zeolites change with exposure to increasingly higher temperatures, All spectra presented in this manuscript will be made available online at "http://aram.ess.sunysb.edu/research.html"; (2) discuss differences in spectral behaviors within and among groups of smectites, sepiolite-palygorskite, kaolinite, chlorites, and zeolites; (3) provide a reference database for future search of the possible existence of dehydrated and/or dehydroxylated phyllosilicates resulting from impact-induced high temperatures on the surface of Mars.

3. Methodology

3.1. Acquisition and Preparation of Samples

[19] Fourteen phyllosilicate and two zeolite samples were selected for this study (Table 1). All samples were purchased from the Clay Minerals Society (CMS) Source Clays repository unless otherwise stated. In addition, two zeolite minerals, mordenite and clinoptilolite, were selected for analysis of their dehydration behavior. Chemical and structure compositions for these samples are summarized in Tables 2 and 3.

[20] To facilitate precise characterization of our samples, a particle size separation method introduced by *Moore and Reynolds* [1989b] was performed on the phyllosilicates and zeolites in order to remove impurities that occur mostly in the >2 μm size fraction [*Moore and Reynolds*, 1989b]. As such, all samples described in this study were prepared to <2 μm size fractions prior to heat treatments. The phyllosilicates and zeolites were then heated under normal atmospheric conditions at 100, 200, 300, 400, 500, 600, 700, 800, and 900°C. The heating duration for each temperature was 24 h. All heated products were stored in a desiccator before spectral measurements.

3.2. Thermogravimetric Analysis

[21] Detailed thermal analysis results for most CMS Source Clay samples have been reported as a part the baseline studies of the source clays [*Guggenheim and Koster van Groos*, 2001]. We performed thermogravimetric analysis on all phyllosili-

Table 2. Summary of Major Elemental Composition[a]

Sample	SiO_2	Al_2O_3	Fe_2O_3	FeO	TiO_2	MgO	CaO	Na_2O	K_2O	P_2O_5	OH/H_2O[b]
SAz-1[c]	51.36	17.20	1.54	n.a.	0.22	5.80	2.71	0.05	0.16	0.01	20.96
STx-1[c]	63.36	16.17	1.09	n.a.	0.24	3.43	1.57	0.28	0.06	0.01	13.78
SWy-2[c]	56.08	20.12	3.99	n.a.	0.08	2.68	1.08	1.34	0.18	0	14.45
SCa-3[d]	55.78	12.47	1.53	n.a.	n.a.	8.55	0.04	2.84	n.a.	n.a.	18.78
Syn-1[c]	47.70	36.75	0.11	n.a.	0.03	0.17	0.05	0.08	0	0	14.91
SBCa-1[e]	51.03	30.71	2.34	0.11	0.57	1.03	1.11	<0.01	0.79	0.12	12.17
SHCa-1[c]	46.11	0.85	0.32	n.a.	0.04	19.77	13.84	1.33	0.14	0	17.60
NAu-1[f]	41.55	6.59	29.07	n.a.	0.02	0.15	2.89	0.02	0.01	n.a.	19.70
NAu-2[f]	49.52	2.74	33.36	n.a.	0.02	0.23	2.06	0.12	0.01	n.a.	11.94
SapCa-2[g]	53.33	4.60	1.19	n.a.	0.09	24.49	1.30	1.19	0.19	n.a.	13.63
KGa-1b[h]	43.98	38.22	0.20	n.a.	1.62	0.06	0.03	0.03	0.02	n.a.	15.84
SepSp-1[i]	55.00	1.40	0.40	0.02	0.04	22.38	1.07	<0.15	0.20	<0.05	19.29
PFl-1[c]	54.33	10.02	3.37	n.a.	0.43	9.52	1.70	0.05	0.78	0.83	18.97
Clinochlore[j]	26.38	29.24	1.64	5.05	n.a.	25.36	n.a.	n.a.	n.a.	n.a.	12.34
27133[k]	67.06	15.51	n.a.	n.a.	n.a.	0.37	3.10	3.92	0.51	n.a.	12.58
27031[l]	61.94	11.97	2.12	n.a.	0.23	1.61	0.91	4.02	1.54	n.a.	15.55

[a]Here n.a., not analyzed.
[b]OH/H_2O takes as total weight loss on ignition (after heating sample to 1000°C).
[c]*Mermut and Faz Cano* [2001].
[d]*Van Olphen and Fripiat* [1979].
[e]Unofficially reported by CMS: http://www.clays.org/SOURCE%20CLAYS/SCdata.html.
[f]*Keeling et al.* [2000].
[g]*Post* [1984].
[h]*Pruett and Webb* [1993].
[i]USGS Digital Spectral Library. http://speclab.cr.usgs.gov/spectral.lib04/DESCRIPT/sepiolite.SepSp-1.html.
[j]*Ballet et al.* [1985].
[k]http://www.handbookofmineralogy.org/pdfs/mordenite.pdf.
[l]*Bish* [1984].

cates and zeolites in order to provide a reference for the IR study of dehydration and dehydroxylation processes. However, it should be pointed out that TGA cannot be compared directly with the IR and XRD results of heated samples because the heating treatment of samples for TGA and other measurements were different. A Netzsch Simultaneous TG-DTA/DSC Apparatus Model STA 449C was used to measure TGA data for all size-separated samples, measuring from 20°C to 1000°C at a heating rate of $10°C \cdot min^{-1}$. An N_2 purge gas system was used to protect samples from atmospheric gases (H_2O and CO_2).

3.3. Acquisition of Powder XRD Patterns

[22] Powder XRD patterns were acquired for all phyllosilicates and zeolites and their heated products in order to confirm their mineralogy and to observe the crystal structural changes of phyllosilicates and zeolites upon heating. XRD data were measured using a Thermo ARL Scintag PAD-X automated powder diffractometer with Cu- Kα radiation, collecting from 5° to 40° 2θ at a 0.6 degree/minute. Samples for XRD analysis were prepared using the smear-mount method with ground sample powders (http://pubs.usgs.gov/of/2001/of01-041/htmldocs/methods/xsslide.htm).

Table 3. Summary of Structural Composition

Sample ID	Structural Composition	Reference[a]
SAz-1	$(Ca_{.39}\ Na_{.36}\ K_{.02})[Al_{2.71}\ Mg_{1.11}\ Fe(III)_{.12}\ Mn_{.01}Ti_{.03}][Si_{8.00}]O_{20}(OH)_4$	1
STx-1	$(Ca_{.27}\ Na_{.04}\ K_{.01})[Al_{2.41}\ Fe(III)_{.09}\ Mn_{tr}Mg_{.71}Ti_{.03}][Si_{8.00}]O_{20}(OH)_4$	1
SWy-2	$(Ca_{.12}\ Na_{.32}\ K_{.05})[Al_{3.01}\ Fe(III)_{.41}\ Mn_{.01}\ Mg_{.54}Ti_{.02}][Si_{7.98}\ Al_{.02}]O_{20}(OH)_4$	1
SCa-3	$(Mg_{.45}Ca_{.15}\ Na_{.26}\ K_{.01})[Al_{2.55}\ Fe(III)_{.12}\ Mn_{tr}\ Mg_{1.31}\ Ti_{.02}][Si_{7.81}Al_{.19}]$ $O_{20}(OH)_4$	1
Syn-1	$(Mg_{.06}Ca_{.04}\ Na_{.12}K_{tr})[Al_{3.99}\ Fe(III)_{tr}\ Mn_{tr}Ti_{tr}][Si_{6.50}\ Al_{1.50}]O_{20}(OH)_4$	1
SBCa-1	$(Mg_{.3}\ Ca_{.16}\ K_{.15})[Al_{3.82}\ Fe(III)_{.18}\ Mn_{tr}\ Ti_{.06}][Si_{6.80}Al_{1.20}]O_{20}(OH)_4$	1
SHCa-1	$(Mg_{.56}\ Na_{.42}\ K_{.05})[Mg_{4.60}\ Li_{1.39}\ Mn_{tr}Ti_{.01}][Si_{7.75}\ Al_{.17}\ Fe(III)_{.05}]O_{20}(OH)_4$	1
NAu-1	$(M^+_{1.05})[Si_{6.98}Al_{1.02}][Al_{0.29}Fe_{3.68}Mg_{0.04}]O_{20}(OH)_4$	2
NAu-2	$(M^+_{0.72})[Si_{7.55}Al_{0.45}][Fe_{3.83}Mg_{0.05}]O_{20}(OH)_4$	2
SapCa-2	$(Ca_{1.14}\ Na_{.79}\ K_{.07})[Mg_{5.98}\ Mn_{.01}\ Ti_{tr}][Si_{7.19}\ Al_{.74}Fe(III)_{.07}]O_{20}(OH)_4$	1
KGa-1b	$(Mg_{.02}Ca_{.01}\ Na_{.01}\ K_{.01})[Al_{3.86}\ Fe(III)_{.02}\ Mn_{tr}Ti_{.11}][Si_{3.83}Al_{.17}]O_{10}(OH)_8$	1
SepSp-1	$(K_{.01})[Mg_{5.54}\ Al_{.35}\ Mn_{.02}\ Fe(II)_{.04}\ Fe(III)_{.14}][Si_{7.90}\ Al_{.1}]O_{20}(OH)_4$	1
PFl-1	$(Mg_{.33}Ca_{.62}\ Na_{.04}\ K_{.13})[Al_{1.50}\ Fe(III)_{.52}\ Fe(II)_{.01}\ Mn_{.01}\ Mg_{1.91}Ti_{.06}][Si_{7.88}$ $Al_{.22}]O_{20}(OH)_4$	1
Clinochlore	$[Si_{3.00}Al_{1.00}]\{Al_{0.96}Fe(II)_{0.48}Fe(III)_{0.14}Mg_{4.30}\}O_{10}(OH)_8$	3
27133	$(Na_{1.11}Ca_{0.48}K_{0.10}Mg_{0.08})Al_{2.16}Si_{9.80}O_{24}\cdot 5.86H_2O$	4
27031	$(Na_{1.80}Ca_{0.23}K_{0.45}Mg_{0.55}Ti_{0.04})Al_{3.25}Si_{14.28}O_{36}\cdot 11.07H_2O$	5

[a]References: 1, Unofficially reported by CMS: http://www.clays.org/SOURCE%20CLAYS/SCdata.html; 2, *Keeling et al.* [2000]; 3, *Ballet et al.* [1985]; 4, http://www.handbookofmineralogy.org/pdfs/mordenite.pdf; 5, *Bish* [1984].

3.4. Infrared Spectroscopic Measurements

[23] Infrared specular reflectance and attenuated total reflectance (ATR) spectra were acquired at Stony Brook University in the Vibrational Spectroscopy Laboratory (VSL) using a Nicolet 6700 FTIR spectrometer.

[24] Specular reflectance peaks are generally referred to as "reststrahlen" features. These occur because the absorption coefficient of a vibrational band is so high that a mirror-like opacity is induced, resulting in strong reflectance from the smooth surface of the samples [*Salisbury*, 1993]. Midinfrared (400–1400 cm^{-1}) and far-infrared specular reflectance (100–600 cm^{-1}) spectra were collected for all phyllosilicates and zeolites and their heated products. A gold-coated first surface mirror was used for the reflectance standard. Each sample was pressed in a Carver Hydraulic Press to create a pellet, 13 mm in diameter and about 3 mm in thickness. Spectra from 400 to 1400 cm^{-1} were acquired using a KBr beamsplitter and a thermoelectrically cooled deuterated L-alanine doped triglycine sulfate (DLaTGS) detector with a KBr window. For each sample, 256 scans in the mid-IR spectral range were recorded with a resolution of 4 cm^{-1}. Spectra from 100 to 600 cm^{-1} were acquired using a Thermo Fisher Solid Substrate beamsplitter and a DLaTGS detector with a polyethylene window. A total of 2048 scans and 4 cm^{-1} resolution were used for the far-IR spectral range. All specular reflectance measurements were collected using a Baseline FT-30 accessory with incidence and reflectance angles of 30°. A purge gas system was used to remove CO_2 and water vapor from the spectrometer.

[25] Attenuated total reflectance (ATR) measurements in the mid-IR (400–4000 cm^{-1}) range were acquired a Nicolet 6700 FTIR spectrometer equipped with a Smart Orbit single bounce ATR accessory with a type II A diamond ATR element which has high refractive index. When IR source radiation enters the ATR element, a total internal reflection occurs and an evanescent wave is formed at the boundary between ATR element and sample. ATR spectra were acquired from unprepared samples rather than pressed pellets because no sample preparation is needed for ATR measurement. The sampling surface is pressed into intimate optical contact with the top surface of ATR crystal and the resulting evanescent wave penetrates only a few microns into the sample. ATR standard was a spectrum with no sample on the ATR element. The resultant spectrum has the similar peak positions to an equivalent absorbance IR spectrum. Because of ATR's easy sample preparation and effectiveness with small grain size, ATR has been considered a potential in situ IR technique for future planetary explorations [*Chemtob and Glotch*, 2007].

4. Results and Interpretations

4.1. Kaolinite-Serpentine Group

4.1.1. Attenuated Total Reflectance Spectra

[26] The ATR spectra of thermally treated KGa-1b kaolinite samples are shown in Figure 1a. OH-stretching vibration bands were observed at ~3620, 3650, 3660, and 3680 cm^{-1} [*Farmer*, 1974] for samples heated from 100°C to 400°C. Dehydroxylation was evidenced by a decrease in intensities of OH-stretching vibration bands at 400°C and the disappearance of these bands at 500°C. Corresponding to the changes in the 3650 cm^{-1} band, the OH-deformation bands at ~910 and ~930 cm^{-1} [*Madejová and Komadel*, 2001] became weaker at 400°C and disappeared at 500°C. The characteristic Si-O stretching vibration bands around 1100, 1020, and 990 cm^{-1} [*Madejová and Komadel*, 2001] disappeared at 500°C and a new peak at ~1050 cm^{-1} formed after the dehydroxylation process was complete. Characteristic Si-O bending vibrations occurring near 400–550 cm^{-1} [*Bishop et al.*, 2008b] began to change significantly at 400°C and completely disappeared when the sample was heated to 500°C. The relatively weak spectral features near 640–800 cm^{-1} were assigned to Si-O bands [*Madejová and Komadel*, 2001], which also changed distinctly upon heating to 400°C.

4.1.2. Specular Reflectance Spectra

[27] The effects of dehydroxylation on the KGa-1b kaolinite reflectance spectra (Figure 1b) were similar to those exhibited in ATR spectra. In both cases, the original spectral features of KGa-1b kaolinite were lost at 400°C, and spectral features from dehydroxylated KGa-1b kaolinite were relatively stable from 500°C to 900°C. Spectral features in the specular reflectance data belonging to the original sample all disappeared at 400°C, but the 400°C ATR spectrum of KGa-1b kaolinite retained decreased original spectral feature at ~525 cm^{-1}.

[28] Upon heating to 400°C, the SiO_4 stretching vibrations occurring at ~1010, ~1060, and ~1130 cm^{-1} [*Bishop et al.*, 2008b] disappeared and were replaced by a new band around 1100 cm^{-1}. This new feature continued to shift toward higher wave numbers upon heating (1076 cm^{-1} at 400°C and 1109 cm^{-1} at 900°C). Other significant changes in the mid-IR region (>400 cm^{-1}) included the disappearance of the OH deformation vibration bands at ~938 cm^{-1} and 908 cm^{-1} [*Bishop et al.*, 2008b] and Si-O bending vibration bands in the range 400–560 cm^{-1} [*Bishop et al.*, 2008b] at 400°C. A new spectral feature appeared in the Si-O bending region at 400°C and this new peak gradually shifted to higher wave numbers (440 cm^{-1} at 400°C and 460 cm^{-1} at 900°C) upon heating. In the far-IR region (<400 cm^{-1}), reflectance peaks occurring at 190, 271, and 345 cm^{-1} were assigned to mixed vibrations which included the Si-O network, octahedral cations, and hydroxyl groups [*Farmer*, 1974]. As with some spectral features described in the mid-IR region, the bands disappeared at 400°C and no new peaks formed at higher temperatures.

4.1.3. Thermogravimetric and X-Ray Diffraction Analysis

[29] TGA and XRD revealed similar behavior to IR spectroscopy for the dehydroxylation process in kaolinite. TGA data for kaolinite (Figure 1c) showed only one significant weight loss from 400°C to 600°C, associated with the loss of hydroxyl groups. The XRD pattern of kaolinite (Figure 1c) at 500°C showed that the 001 peak disappeared, indicated that the layer structure of kaolinite has been destroyed by 500°C. TGA data for this corresponding temperature range showed a 25 wt% loss due to evolution of H_2O from OH groups.

4.2. Smectite Group

4.2.1. Montmorillonite

[30] Four montmorillonite samples of various origins and compositions are discussed in this section. A fifth sample, Syn-1 mica-montmorillonite is discussed later. Although Syn-1 is listed by the Clay Minerals Society as a synthetic

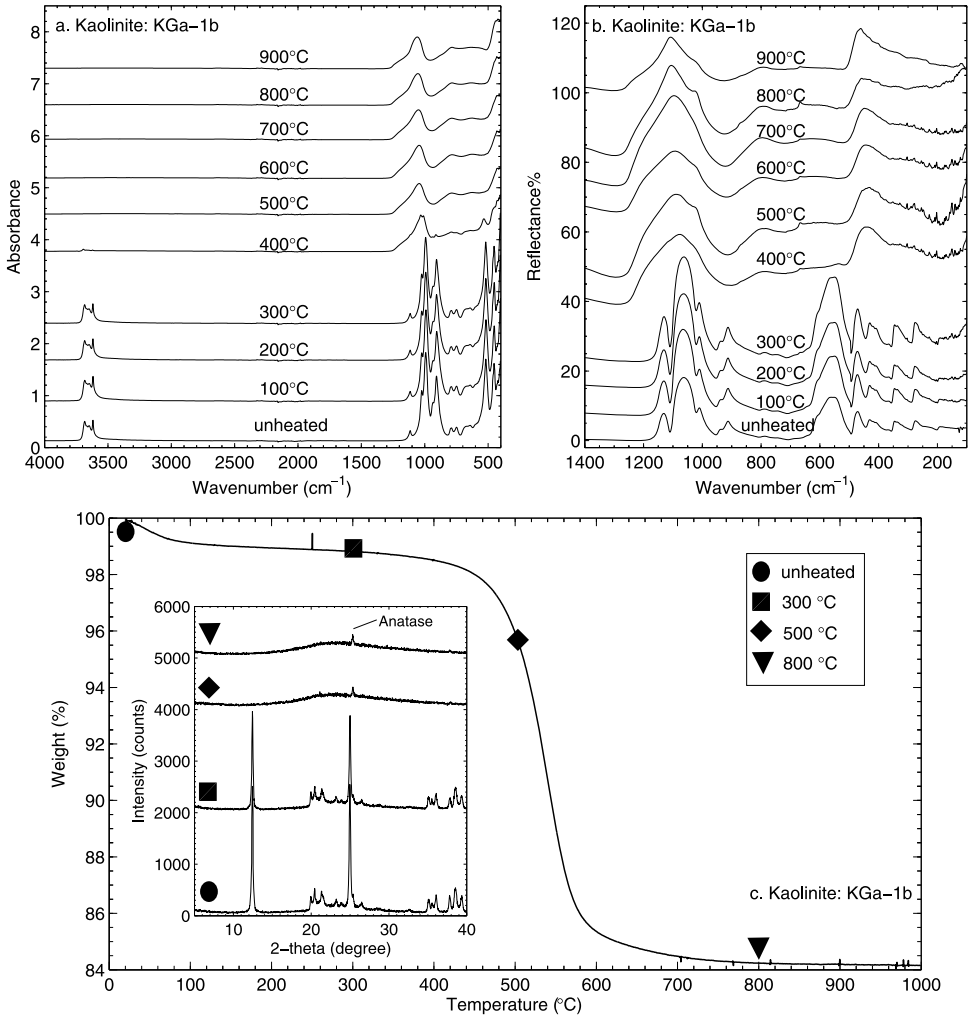

Figure 1. (a) The 400–4000 cm^{-1} ATR spectra of kaolinite (KGa-1b) calcined at various temperatures. (b) The 100–1500 cm^{-1} specular reflectance spectra of kaolinite (KGa-1b) calcined at various temperatures. Linear vertical offset is applied to the spectra for clarity. (c) TGA plots and X-ray diffraction profiles (offset) of KGa-1b kaolinite.

mica-montmorillonite, previous study [*Kloprogge et al.*, 1999a] indicates that both its chemical composition and spectral features are close to those for beidellite. Therefore, data for Syn-1 will be discussed with the beidellite sample SBCa-1.

4.2.1.1. Attenuated Total Reflectance Spectra

[31] Dehydroxylation of SAz-1 montmorillonite, evidenced by disappearance of its Al-Al-OH deformation band (912 cm^{-1}), Al-Mg-OH deformation band (837 cm^{-1}), and OH stretching bands (3610 cm^{-1}, 3398 cm^{-1}) [*Madejová and Komadel*, 2001], occurred at 500°C (Figure 2a). The 500°C spectrum of SAz-1 retained a weak 1631 cm^{-1} H-O-H bending band but this feature disappeared in the 600°C spectrum. Over the same temperature range the 509 cm^{-1} Al-O-Si deformation band [*Madejová and Komadel*, 2001] disappeared. Beginning at a temperature of 500°C, the Si-O stretching band at 972 cm^{-1} became broad and was eventually replaced by two bands at 922 cm^{-1} and 1059 cm^{-1} above 700°C. Another Si-O stretching band (longitudinal mode) at ~1126 cm^{-1} [*Madejová and Komadel*, 2001] was relatively stable but it disappeared at 800°C. An additional new strong feature began to develop at ~780 cm^{-1} when SAz-1 montmorillonite was heated to 800°C.

[32] The SCa-3 montmorillonite showed similar spectral behavior to SAz-1 montmorillonite (Figure 2b). The OH-stretching bands (~3610 cm^{-1} and ~3398 cm^{-1}) disappeared at 600°C and the H-O-H bending band (~1630 cm^{-1}) disappeared at 700°C. The Al-Al-OH deformation band, Al-Mg-OH deformation band, and Al-O-Si deformation band (~910 cm^{-1}, ~830 cm^{-1}, and ~505 cm^{-1}, respectively) disappeared at 500°C. The Si-O stretching band (~970 cm^{-1}) broaded and was replaced by two bands (~1050 cm^{-1} and ~920 cm^{-1}) at 700°C. The Si-O stretching band (longitudinal mode) gradually shifted to higher wave numbers (~1109 cm^{-1} at room temperature to ~1138 cm^{-1} at 700°C) and it disappeared at 800°C. Finally, a new spectral feature at ~780 cm^{-1} formed at 800°C.

[33] Most OH groups were removed from the STx-1 structure by 500°C, evidenced by disappearance of the Al-Mg-OH deformation (~842 cm^{-1}), Al-Al-OH deformation (~914 cm^{-1}), and OH stretching (3624 cm^{-1} and 3340 cm^{-1}) bands (Figure 2c). The 515 cm^{-1} Al-O-Si deformation band

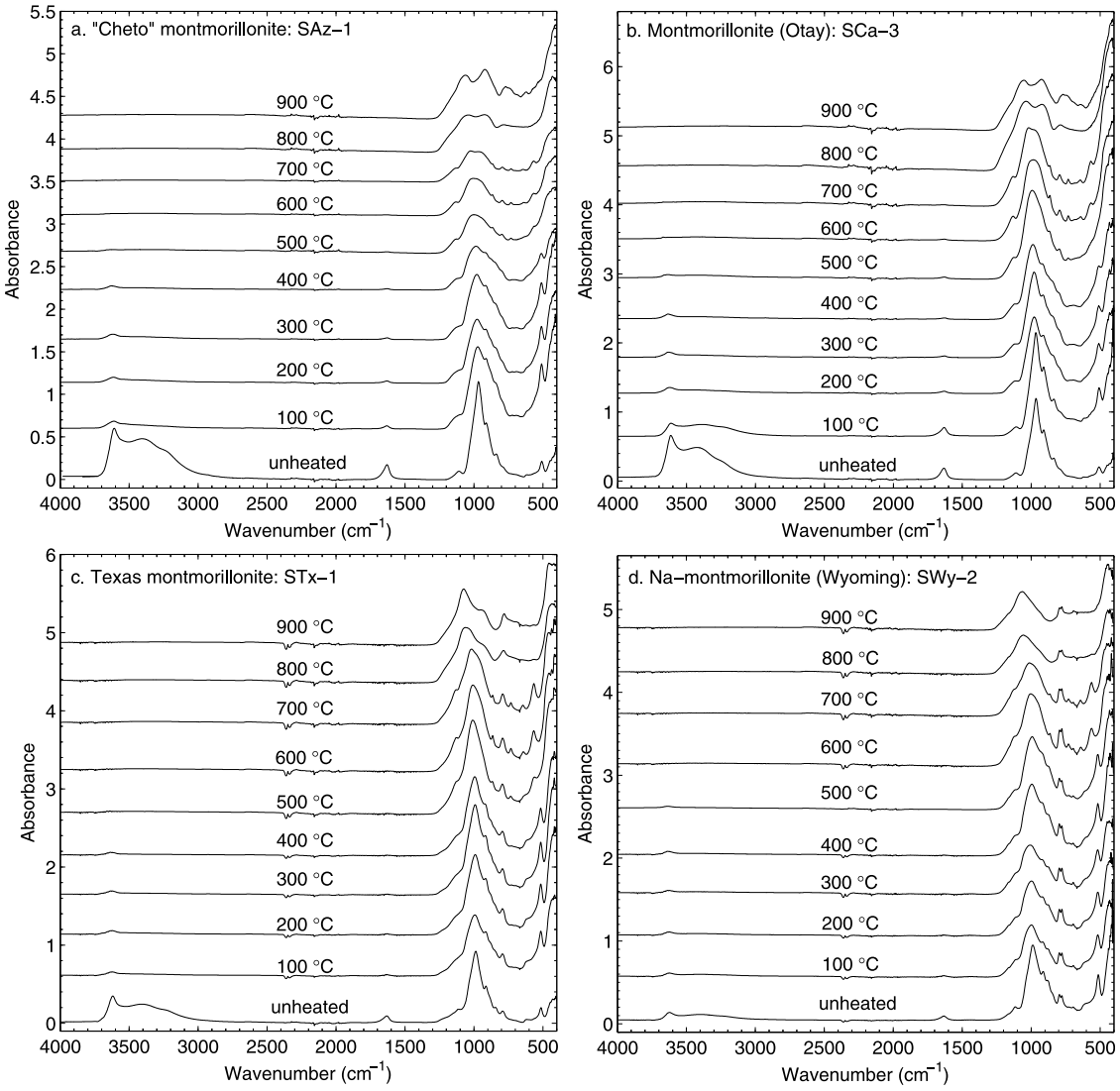

Figure 2. The 400–4000 cm^{-1} ATR spectra of (a) "Cheto" montmorillonite (SAz-1), (b) montmorillonite (Otay) (SCa-3), (c) Texas montmorillonite (STx-1), and (d) Na-montmorillonite (Wyoming) (SWy-2) calcined at various temperatures. Linear vertical offset is applied to the spectra for clarity.

disappeared at 500°C, and a new band at ~567 cm^{-1} began to develop at 600°C and disappeared at 800°C. The Si-O stretching band experienced a distinct shift toward higher frequencies at 500°C heating (~993 cm^{-1} at room temperature, ~1074 cm^{-1} at 900°C) and the weak Si-O stretching (longitudinal mode) band at ~1126 cm^{-1} disappeared after 800°C heating. The spectral feature at ~792 cm^{-1} was assigned to Si-O stretching of cristobalite [*Madejová and Komadel*, 2001] and it showed no changes on heating.

[34] The OH-stretching (~3624 cm^{-1}, ~3390 cm^{-1}), Al-Al-OH deformation (~914 cm^{-1}), and Al-Fe-OH deformation (~881 cm^{-1}) bands disappeared at 600°C, indicating the loss of OH groups (Figure 2d). Upon heating to 800°C, the 989 cm^{-1} Si-O stretching band of SWy-2 montmorillonite shifted to higher frequencies, to ~1065 cm^{-1} at 900°C. The 1117 cm^{-1} Si-O stretching (longitudinal mode) band became weaker with an increase in temperature and it disappeared above 800°C. The 513 cm^{-1} Al-O-Si deformation band disappeared at 600°C and a new peak at ~561 cm^{-1} began to grow at this temperature. This new peak disappeared at 800°C. The 777 cm^{-1} and 796 cm^{-1} bands were assigned to Si-O stretching modes of quartz admixture [*Madejová and Komadel*, 2001], and were not affected by the heating treatment.

4.2.1.2. Specular Reflectance Spectra

[35] SAz-1 and SCa-3 montmorillonites had similar reflectance spectral behaviors when they were heated (Figures 3a and 3b), and three stages of spectral change were observed. There was no distinct spectral change from 100°C to 400°C, although the spectra showed minor increases in intensity and high-frequency shifting of the Si-O stretching (longitudinal mode) band (1117 cm^{-1} to 1140 cm^{-1} for SAz-1, 1114 cm^{-1} to 1138 cm^{-1} for SCa-3). From 500°C to 700°C, the Si-O stretching region was dominated by two broad peaks (~1153 cm^{-1} and ~1061 cm^{-1} for SAz-1, ~1149 cm^{-1} and ~1057 cm^{-1} for SCa-3). The Si-O bending region showed more significant changes than the Si-O stretching region over this temperature range. The original doublet feature at

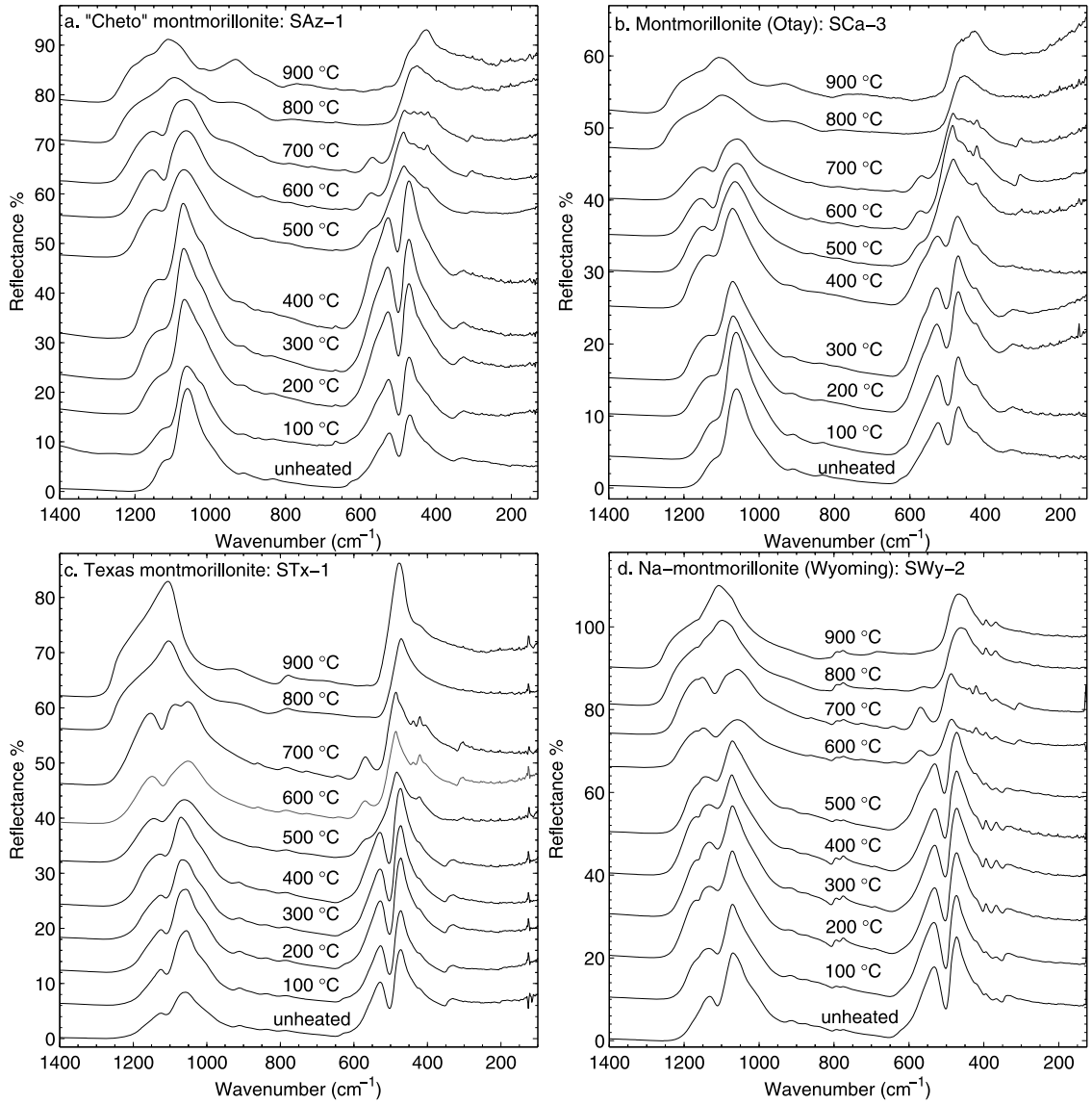

Figure 3. (a) The 130–1400 cm^{-1} specular reflectance spectra of "Cheto" montmorillonite (SAz-1) calcined at various temperatures. (b) The 130–1400 cm^{-1} specular reflectance spectra of montmorillonite (Otay) (SCa-3) calcined at various temperatures. (c) The 100–1400 cm^{-1} specular reflectance spectra of Texas montmorillonite (STx-1) calcined at various temperatures. (d) The 125–1400 cm^{-1} specular reflectance spectra of montmorillonite (Wyoming) (SWy-2) calcined at various temperatures. Linear vertical offset is applied to the spectra for clarity.

~500 cm^{-1} was completely lost and was replaced by a strong band with complex shoulder spectral features (~486 cm^{-1} for SAz-1, ~487 cm^{-1} for SCa-3). The original 327 cm^{-1} spectral feature in the far-IR region disappeared and a new peak formed at ~302 cm^{-1} for both SAz-1 and SCa-3 samples. After heating to 800°C and 900°C, multiple spectral features for SAz-1 and SCa-3 combined to form a single strong peak for both Si-O stretching and bending regions. A new strong band (~933 cm^{-1} for SAz-1, ~927 cm^{-1} for SCa-3) also developed in this temperature range.

[36] The reflectance spectra of STx-1 montmorillonite and its heating products are displayed in Figure 3c. The 500°C heat treatment produced significant spectral changes. The doublet feature at ~500 cm^{-1} caused by Si-O bending modes and the ~330 cm^{-1} peak in the far-IR region disappeared. Two bands at ~1100 cm^{-1} due to Si-O stretching vibrations shifted away from each other, and new spectral features caused by heating were observed at ~565 cm^{-1}, ~484 cm^{-1}, and 302 cm^{-1}. Upon heating to 800°C, all new spectral features formed at lower temperatures disappeared, and two strong reflectance bands at ~1105 cm^{-1} and ~470 cm^{-1} dominated the mid-IR and far-IR regions of the STx-1 montmorillonite spectra.

[37] In the case of the Swy-2 montmorillonite, two spectral features associated with Si-O stretching around 1070 cm^{-1} and 1130 cm^{-1} broadened and shifted away from each other at 600°C and they were replaced by a band near 1107 cm^{-1} (Figure 3d) at 800°C. A new shoulder feature near 1130 cm^{-1} formed at 200°C and disappeared at 500°C. New reflectance peaks at ~568 cm^{-1} and ~484 cm^{-1} appeared at 600°C and the

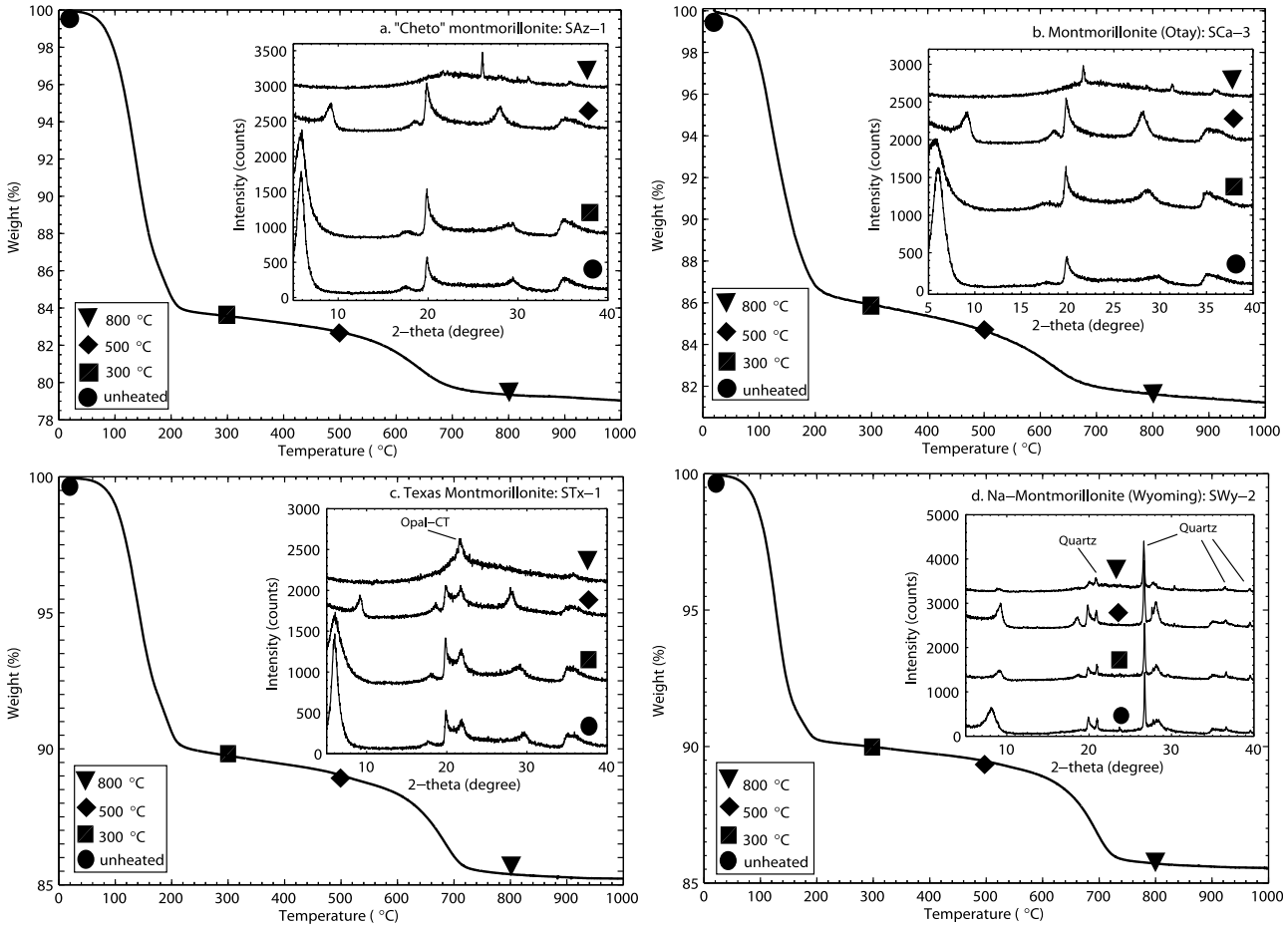

Figure 4. TGA plots and X-ray diffraction profiles (offset) of (a) SAz-1 "Cheto" montmorillonite, (b) SCa-3 montmorillonite (Otay), (c) STx-1 Texas montmorillonite, and (d) SWy-2 Na-montmorillonite (Wyoming).

Al-O-Si deformation (~534 cm^{-1}) and Si-O-Si deformation (474 cm^{-1}) bands disappeared completely at this temperature. However, these new peaks disappeared at 800°C and a new strong reflectance band appeared at ~462 cm^{-1}. Distinct spectral changes also occur at 600°C and 800°C in the far-IR region (<400 cm^{-1}), evidenced by disappearance of the original 335 cm^{-1} feature and formation of a new 302 cm^{-1} band at 600°C. All of these spectral features disappeared at 800°C. Spectral features at 775 cm^{-1}, 795 cm^{-1}, 393 cm^{-1}, and 366 cm^{-1} are related to quartz admixture [*Madejová and Komadel*, 2001] and they persisted through the dehydration and dehydroxylation of SWy-2 montmorillonite.

4.2.1.3. Thermogravimetric and X-Ray Diffraction Analysis

[38] SAz-1 "Cheto" montmorillonite and SCa-3 montmorillonite (Otay) have similar thermal behaviors, related to their identical structures and similar chemical compositions [*Grim and Kulbicki*, 1961]. Two distinct changes in the TGA curves (Figures 4a and 4b) were observed for both montmorillonites, consistent with the fact that they contain both molecular H_2O and hydroxyl groups in their structures. The dehydration processes, as evidenced by abrupt weight losses at ~100°–200°C, indicate that both samples began to lose H_2O rapidly from the beginning of heat treatment. Both montmorillonites began to lose their structural OH groups gradually from 600°C to 700°C. XRD data showed that these two montmorillonites retained their original 001 reflection positions at 300°C, and the TGA results indicated that most of their interlayer H_2O molecules were lost by 200°C. The reason may be related to the details of our experimental process for both phyllosilicates and zeolites as heated samples were not protected from rehydration during XRD measurements [e.g., *Gavin and Chevrier*, 2010]. The XRD results showed that these two montmorillonites were capable of reabsorbing H_2O from the air after heating to 300°C. The d-spacing of the 001 reflections decreased at 500°C showing structural collapse, and at 800°C the 001 reflections disappeared, indicating that the layer structures of SAz-1 and SCa-3 montmorillonites had been destroyed.

[39] STx-1 montmorillonite (Figure 4c) has a lower overall content (~14%) of OH and H_2O (Table 2) in its structure than SAz-1 (~21%) and SCa-3 (~19%), due primarily to differences in exchangeable-cation composition. The STx-1 montmorillonite dehydroxylated more rapidly at higher temperatures (~700°C) than the other two montmorillonites (~650°C). Otherwise, the dehydration and dehydroxylation processes of STx-1 montmorillonite manifested in TGA and XRD results (Figure 4c) are similar to those of SAz-1 and SCa-3 montmorillonites.

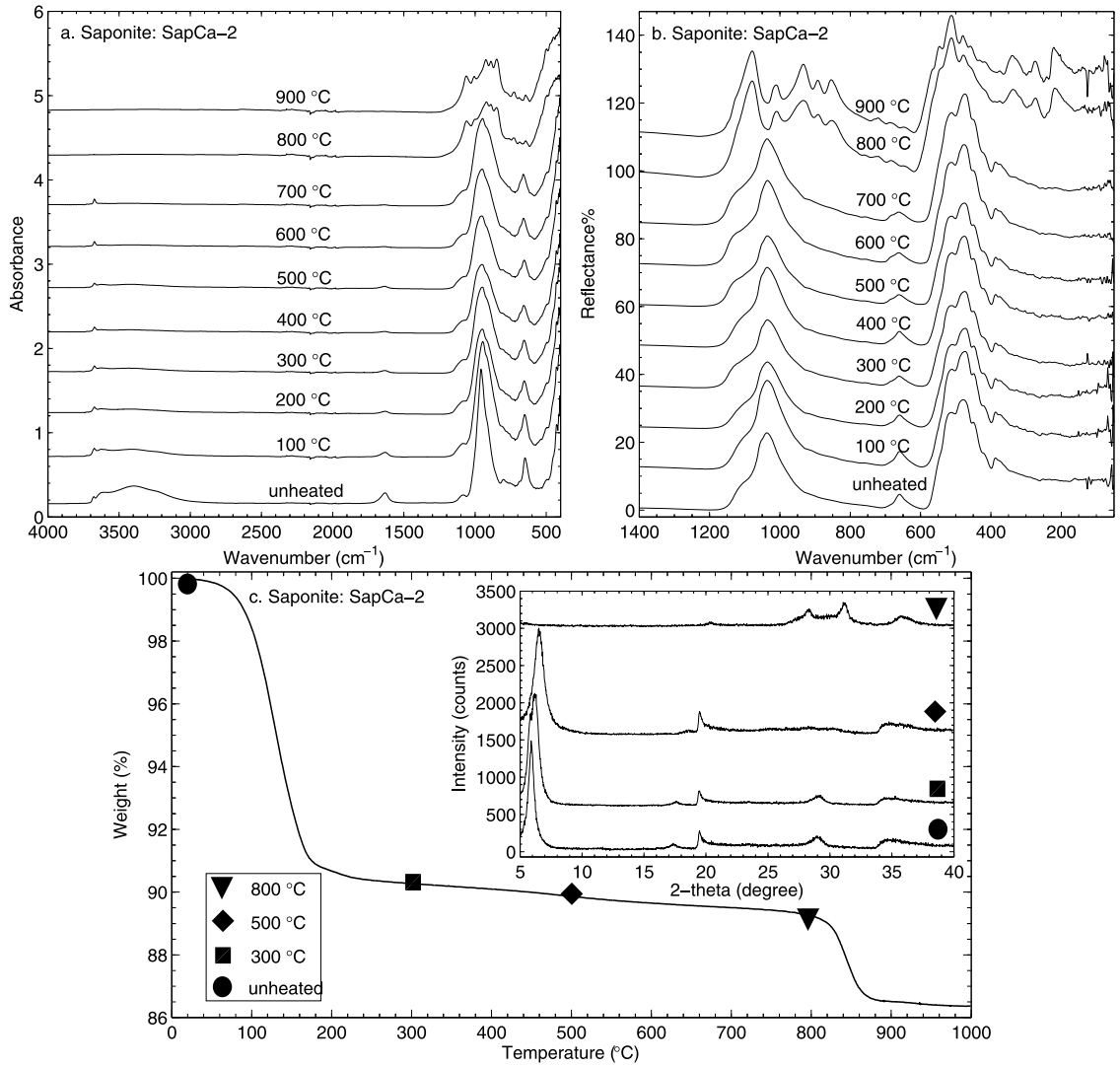

Figure 5. (a) The 400–4000 cm^{-1} ATR spectra of saponite (SapCa-2) calcined at various temperatures. (b) The 50–1400 cm^{-1} specular reflectance spectra of saponite (SapCa-2) calcined at various temperatures. Linear vertical offset is applied to the spectra for clarity. (c) TGA plots and X-ray diffraction profiles (offset) of SapCa-2 saponite.

[40] SWy-2 montmorillonite is the most stable among the four montmorillonites examined here. The 001 reflection of SWy-2 remained as a weak peak at 800°C (Figure 4d), indicating that dehydroxylation at this point was incomplete.

4.2.2. Saponite

4.2.2.1. Attenuated Total Reflectance Spectra

[41] The spectral features at ~3678 cm^{-1}, ~3625 cm^{-1}, and ~3410 cm^{-1} were assigned to Mg-O-H stretching, Al-O-H stretching, and H-O-H stretching modes, respectively [*Van der Marel and Beutelspacher*, 1976]. The Al-O-H stretching and H-O-H stretching bands disappeared at 200°C but the Mg-O-H stretching feature persisted to 700°C (Figure 5a), indicating that most of the OH groups in the saponite (SapCa-2) structure were lost around 700°C. Correspondingly, the Mg-OH libration band at ~650 cm^{-1} [*Van der Marel and Beutelspacher*, 1976] was observed only to 700°C. The H_2O bending band near 1630 cm^{-1} disappeared at 600°C. No distinct change occurred for Si-O stretching bands (~1080 cm^{-1} and ~950 cm^{-1}) until 700°C. Upon heating to 800°C, the original Si-O stretching bands disappeared and were replaced by multiple spectral features between 850 and 1200 cm^{-1}, and similar changes were seen between 600 cm^{-1} and 750 cm^{-1} at this temperature.

4.2.2.2. Specular Reflectance Spectra

[42] Similar to the ATR spectra for SapCa-2 saponite, the reflectance spectra did not show any distinct change until 700°C (Figure 5b), although the intensity of the weak Si-O stretching band at ~1115 cm^{-1} increased gradually with temperature. The 800°C and 900°C reflectance spectra of saponite exhibited completely different features from those at 700°C. Spectral ranges from 800 cm^{-1} to 1200 cm^{-1} and from 200 cm^{-1} to 600 cm^{-1} were both dominated by complex multiple bands at 800°C and 900°C.

4.2.2.3. Thermogravimetric and X-Ray Diffraction Analysis

[43] TGA data (Figure 5c) for SapCa-2 saponite showed that most interlayer H_2O molecules were lost below 150°C, whereupon saponite remained relatively stable until

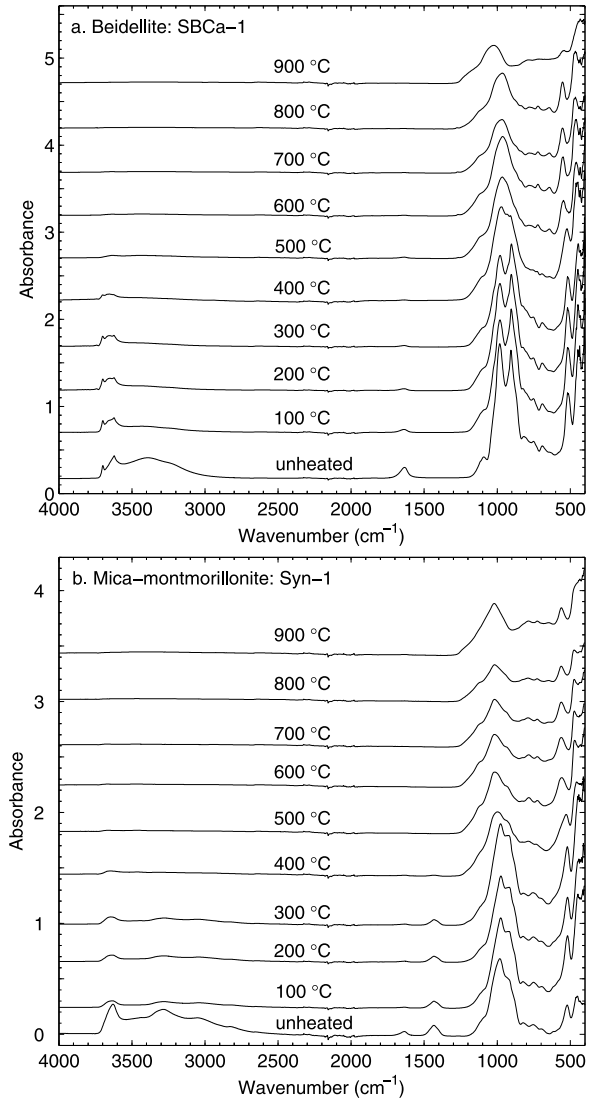

Figure 6. (a) The 400–4000 cm^{-1} ATR spectra of beidellite (SBCa-1) calcined at various temperatures. (b) The 400–4000 cm^{-1} ATR spectra of mica-montmorillonite (Syn-1) calcined at various temperatures. Linear vertical offset is applied to the spectra for clarity.

800°C. From 800°C to 850°C, a significant weight loss was observed, associated with dehydroxylation of saponite. XRD data (Figure 5c) show that the layer structure of saponite was not affected distinctly until ~500°C. Above this temperature, a new well-crystallized phase was formed at 800°C, just before the onset of the dehydroxylation process as evidenced by TGA data. This high-temperature phase of saponite has been determined by previous studies and confirmed in this study [e.g., *Kulbicki*, 1959] to be enstatite ($MgSiO_3$), which accounts for the nature of the high-temperature spectral data.

4.2.3. Beidellite

4.2.3.1. Attenuated Total Reflectance Spectra

[44] Dehydroxylation of SBCa-1 beidellite resulted in the disappearance of its OH-stretching bands (~3697 cm^{-1}, ~3610 cm^{-1}, and ~3400 cm^{-1}) and the Al-O-H libration band (~906 cm^{-1}) at ~500°C (Figure 6a). The 1090 cm^{-1} Si-O stretching (longitudinal mode) [*Kloprogge et al.*, 1998] band gradually became weaker as temperature increased. The 980 cm^{-1} Si-O stretching band was stable until 800°C and was replaced by a new spectral feature (~1024 cm^{-1}) at 900°C. The 519 cm^{-1} Al-O-Si bending band began to shift gradually toward higher wave numbers (~524 cm^{-1} at 400°C and ~553 cm^{-1} at 800°C) after heating to 400°C and it was replaced by a weak band at ~547 cm^{-1} at 900°C.

[45] The dehydroxylation of Syn-1 montmorillonite was essentially complete around 600°C, as evidenced by the disappearance of the OH-stretching band at ~3629 cm^{-1} in the 600°C ATR spectrum (Figure 6b). The 1635 cm^{-1} H_2O bending feature Syn-1 montmorillonite disappeared at 400°C. The 920 cm^{-1} Al-Al-OH deformation band decreased in intensity at 400°C and disappeared after 700°C heating. The Si-O stretching band at ~976 cm^{-1} disappeared at 400°C and was replaced by a broader band around 1018 cm^{-1}, which remained until 900°C. The 518 cm^{-1} feature associated with Si-O-Al bending mode decreased in intensity at 400°C and this weaker band shifted to 562 cm^{-1} at temperatures > 400°C. Syn-1 montmorillonite has ammonium in its interlayer [*Kloprogge et al.*, 1999a] and several spectral changes related to ammonium were observed on heating. Features in the 3300–2800 cm^{-1} and near 1433 cm^{-1} were assigned to stretching and deformation vibrations of NH_4^+, respectively [*Madejová and Komadel*, 2001]. The ammonium was lost at temperatures above 500°C based on the disappearance of these spectral bands.

4.2.3.2. Specular Reflectance Spectra

[46] Significant spectral changes in SBCa-1 beidellite began at 400°C (Figure 7a). The 1125 cm^{-1} and 1057 cm^{-1} Si-O stretching bands began to shift away from each other (1134 cm^{-1} and 1045 cm^{-1} at 400°C), the 1015 cm^{-1} Si-O stretching shoulder band disappeared, the 910 cm^{-1} Al-O-H libration band disappeared; the 550 cm^{-1} Si-O-Al bending band [*Kloprogge et al.*, 1998] shifted to higher wave numbers (shifting to 567 cm^{-1} at 500°C), and weak bands in the range 100 cm^{-1} to 400 cm^{-1} were all lost after 400°C heating. A new spectral feature near 300 cm^{-1} formed at 500°C. Then all spectral features, including both the original features and new bands developed at lower temperatures, were completely lost at 900°C. The 900°C reflectance spectrum of SBCa-1 beidellite was dominated by four spectral features at ~1097 cm^{-1}, ~796 cm^{-1}, 553 cm^{-1}, and 462 cm^{-1}.

[47] The Si-O stretching bands at ~1122 cm^{-1} and ~1053 cm^{-1} continued to shift away from each other (1142 cm^{-1} and 1045 cm^{-1} at 800°C) as temperature increased and at 900°C they were replaced by a broad band centered near 1097 cm^{-1} (Figure 7b). The weak Al-O-H libration band (~918 cm^{-1}) was lost after 400°C heating. The 545 cm^{-1} Si-O-Al bending band shifted to 570 cm^{-1} after 500°C and remained stable to 900°C. The Si-O bending bands at ~480 cm^{-1} and ~420 cm^{-1} shifted slightly away from each other (484 cm^{-1} and 406 cm^{-1} at 900°C) with increasingly higher temperatures and they existed in the 900°C spectrum as features with comparable intensities.

4.2.3.3. Thermogravimetric and X-Ray Diffraction Analysis

[48] SBCa-1 beidellite and Syn-1 mica-montmorillonite both have high Al contents and comparable concentrations of OH and H_2O in their structures (Table 2). SBCa-1 exhibited two significant weight losses at ~150°C and ~450°–550°C (Figure 8a), but XRD data indicated that its layer structure

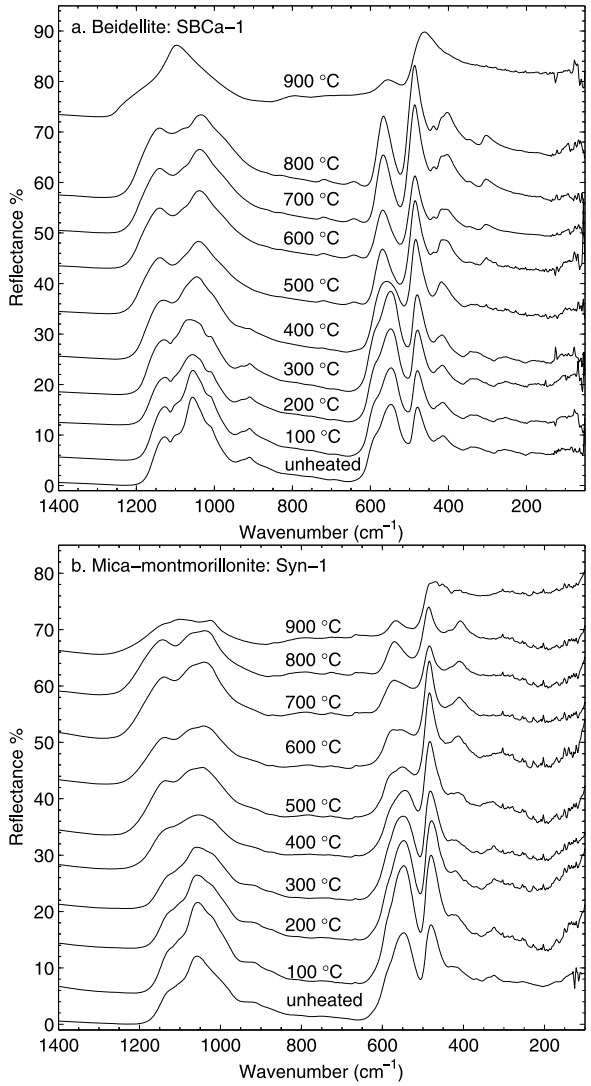

Figure 7. (a) The 50–1400 cm^{-1} specular reflectance spectra of beidellite (SBCa-1) calcined at various temperatures. (b) The 100–1400 cm^{-1} specular reflectance spectra of mica-montmorillonite (Syn-1) calcined at various temperatures. Linear vertical offset is applied to the spectra for clarity.

was stable to at least 800°C. This conflict suggests that dehydration and dehydroxylation did not destroy the crystal structure by this temperature, and beidellite did not transform to an amorphous phase as montmorillonites did at 800°C. Syn-1 mica-montmorillonite experienced the first weight loss in its TGA curve (Figure 8b) from room temperature to ~150°C and the second significant weight loss occurred between 400°C and 650°C. The structure of Syn-1 mica-montmorillonite was also intact to 800°C based on XRD data.

4.2.4. Hectorite

4.2.4.1. Attenuated Total Reflectance Spectra

[49] Heating to 600°C resulted in disappearance of the H-O-H bending band at ~1624 cm^{-1} and OH-stretching bands at 3400–3680 cm^{-1} (Figure 9a). The single Si-O stretching band at ~960 cm^{-1} broadened at 400°C and split into multiple spectral peaks after 500°C heating. Beginning at 600°C, significant change was observed for the Si-O stretching region and a series of new bands (~850–1060 cm^{-1}) formed over this temperature range remained until 900°C. The ~650 cm^{-1} and ~700 cm^{-1} spectral features were assigned to Mg-OH deformation of SHCa-1 hectorite and the in-plane CO_3^{2-} bending mode of calcite (existing as a contaminant in the hectorite sample), respectively [*Kloprogge et al.*, 2000]. They both disappeared in the 600°C spectrum and were replaced by two small bands at ~670 cm^{-1} and ~630 cm^{-1} after 600°C heating.

4.2.4.2. Specular Reflectance Spectra

[50] Specular reflectance results for SHCa-1 hectorite showed that distinct changes due to heating took place around 500°C (Figure 9b). Upon heating to 500°C, the 1047 cm^{-1} Si-O stretching band and the 476 cm^{-1} Si-O bending band both split into multiple bands between 900 and 1070 cm^{-1} and 400–500 cm^{-1} and a series of new spectral features formed in the far-IR region between 200 and 350 cm^{-1}.

4.2.4.3. Thermogravimetric and X-Ray Diffraction Analysis

[51] Dehydration and dehydroxylation processes for SHCa-1 hectorite begin at ~150°C and from ~650°C to ~800°C, respectively (Figure 9c). However, a unique weight loss around 770°C may be caused by dolomite decarbonation [*Guggenheim and Van groos*, 2001]. XRD data show calcite in hectorite even after acid treatment, and the presence of calcite and dolomite may contribute to weight-loss events

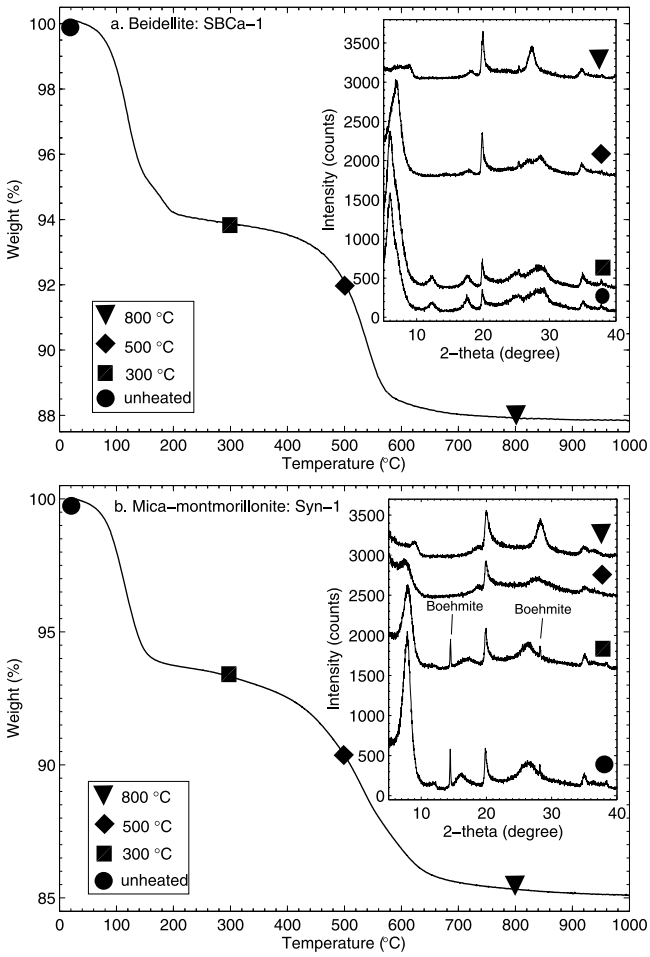

Figure 8. TGA plots and X-ray diffraction profiles (offset) of (a) SBCa-1 beidellite and (b) Syn-1 mica-montmorillonite.

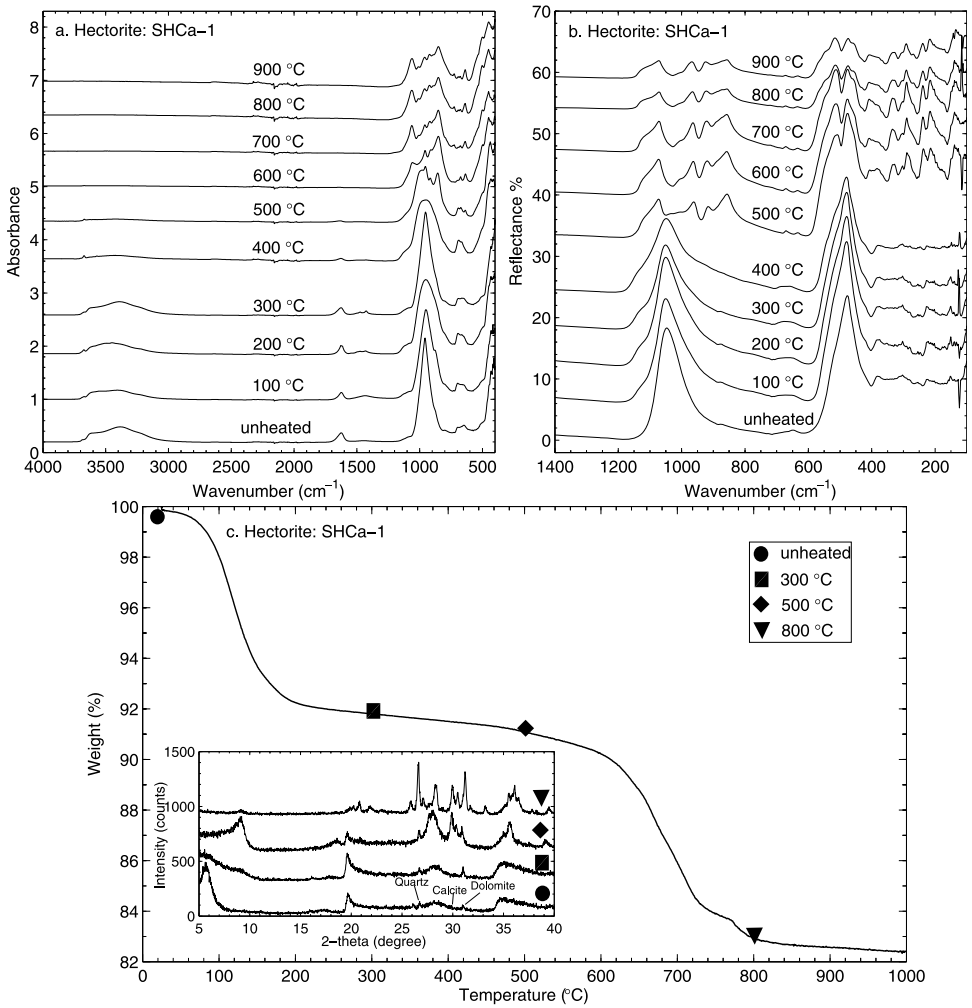

Figure 9. (a) The 400–4000 cm^{-1} ATR spectra of hectorite (SHCa-1) calcined at various temperatures. (b) The 100–1400 cm^{-1} specular reflectance spectra of hectorite (SHCa-1) calcined at various temperatures. Linear vertical offset is applied to the spectra for clarity. (c) TGA plots and X-ray diffraction profiles (offset) of SHCa-1 hectorite.

observed by TGA. Compared with the untreated sample, the 500°C XRD pattern of hectorite showed collapse of original layer structure and formation of a new phase. The 800°C XRD pattern of hectorite was consistent with well-ordered enstatite. The transformation from hectorite to enstatite at high temperatures has been summarized previously [e.g., *Green et al.*, 1970; *Kloprogge et al.*, 2000].

4.2.5. Nontronite

4.2.5.1. Attenuated Total Reflectance Spectra

[52] NAu-1 and NAu-2 nontronites are both high-Fe dioctahedral smectites. The major chemical difference between them is a higher Al content in NAu-1 nontronite [*Keeling et al.*, 2000].

[53] The first distinct ATR spectral change in NAu-1 nontronite occurred at 400°C (Figure 10a). Most spectral features related to OH groups [*Frost and Kloprogge*, 2000; *Frost et al.*, 2002], including the Fe-Fe-OH stretching band (~3560 cm^{-1}), OH stretching of H_2O (~3400 cm^{-1}), Al-Fe-OH deformation band (~908 cm^{-1}), Fe-Fe-OH deformation band (~808 cm^{-1}), and the Mg-Fe-OH deformation band (~742 cm^{-1}), disappeared upon heating to 400°C. The 484 cm^{-1} Si-O-Fe bending band also disappeared at 400°C. The 1630 cm^{-1} H_2O bending band became weak at 400°C and was lost at 500°C. A new spectral feature at ~790 cm^{-1} developed at 500°C and remained until 900°C. The Si-O stretching band near 1000 cm^{-1} showed a gradual shift to higher wave numbers (975 cm^{-1} at room temperature and 1053 cm^{-1} at 900°C) as temperature increased. In addition, absorption features at ~3695 cm^{-1} and ~3620 cm^{-1} were related to kaolinite, which existed in the NAu-1 sample as a contaminant [*Keeling et al.*, 2000], and both bands disappeared at 400°C.

[54] NAu-2 nontronite exhibited spectral behavior upon heating similar to NAu-1 nontronite although the spectra had slightly different band positions (Figure 10b). Most of the original spectral features of NAu-2 nontronite disappeared at 400°C or 500°C; the Si-O stretching band around 1000 cm^{-1} continued to shift toward higher wave numbers during the heat treatment and new spectral features developed in the range 500 cm^{-1} to 800 cm^{-1} upon heating to 600°C. Based on the spectral results, there is no kaolinite in the NAu-2 nontronite.

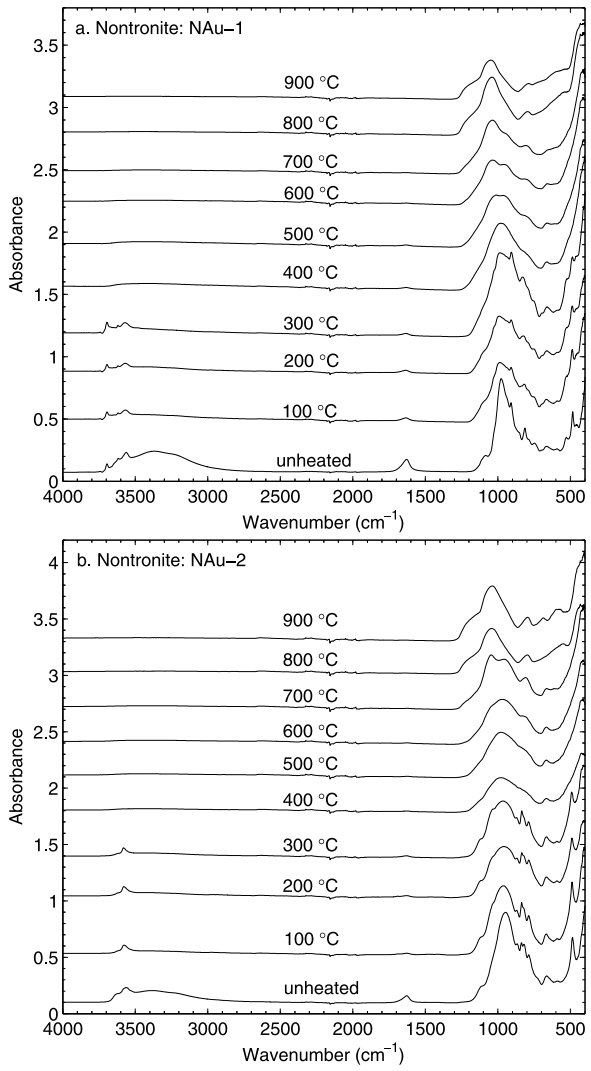

Figure 10. (a) The 400–4000 cm^{-1} ATR spectra of nontronite (NAu-1) calcined at various temperatures. (b) The 400–4000 cm^{-1} ATR spectra of nontronite (NAu-2) calcined at various temperatures. Linear vertical offset is applied to the spectra for clarity.

4.2.5.2. Specular Reflectance Spectra

[55] Two distinct spectral changes took place around 300°–400°C and 700°–800°C for both nontronite samples (Figures 11a and 11b) as they were heated. The spectral features in the 200–400 cm^{-1} region related to mixed vibrations of the Si-O network [*Farmer*, 1974] and bands around 850 cm^{-1} associated with OH deformation modes [*Frost and Kloprogge*, 2000; *Frost et al.*, 2002] were all lost after 400°C heating. Multiple Si-O bending bands near 500 cm^{-1} disappeared and a new band formed (~460 cm^{-1} for NAu-1 nontronite, ~470 cm^{-1} for NAu-2 nontronite). The Si-O stretching bands of NAu-1 and NAu-2 nontronites near 1050 cm^{-1} displayed changes similar to each other at 400°C by combining and forming one singe band. After 800°C, these new bands in the Si-O stretching and bending regions both shifted slightly to higher frequencies and new spectral features developed in the range 600–800 cm^{-1}. In addition, a weak spectral band in the far-IR region (<400 cm^{-1}) around 310 cm^{-1} appeared for both NAu-1 and NAu-2 nontronites at 400°C and it remained until 900°C.

4.2.5.3. Thermogravimetric and X-Ray Diffraction Analysis

[56] TGA data for nontronite samples NAu-1 and NAu-2 showed their first distinct weight loss below ~200°C and the loss occurred from ~400°C to ~600°C (Figures 12a and 12b). XRD data for the nontronites indicated that their layer structures were destroyed by 800°C. Simultaneously, new features appeared in the XRD patterns (~35°, 2θ) for both NAu-1 and NAu-2 nontronites, indicating crystallization of new phases.

4.3. Chlorite Group

4.3.1. Attenuated Total Reflectance Spectra

[57] Upon heating to 500°C, OH-stretching bands (~3678 cm^{-1}, ~3535 cm^{-1}, ~3373 cm^{-1}) disappeared

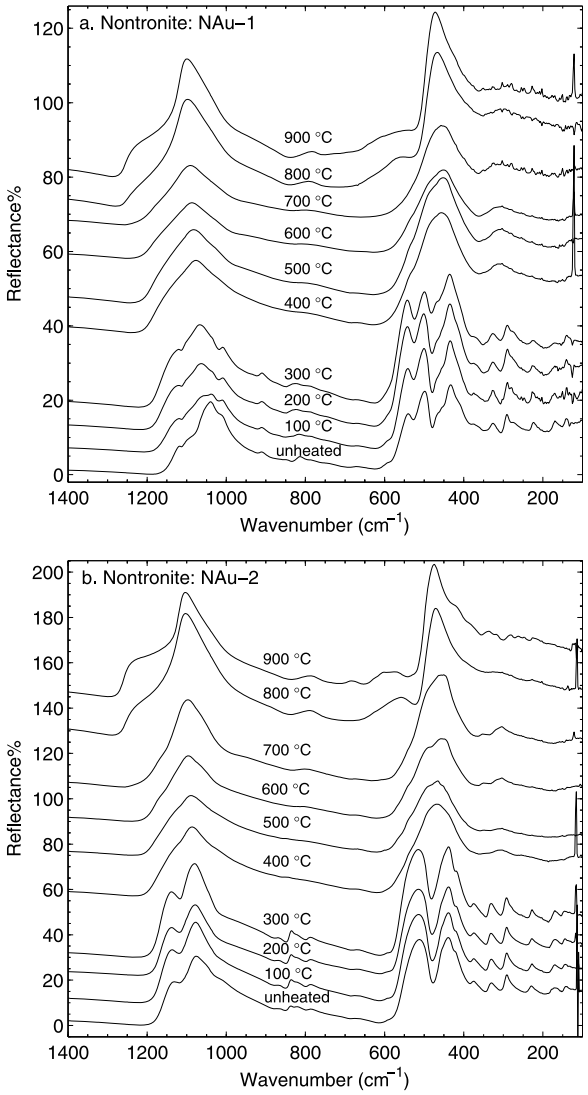

Figure 11. (a) The 100–1400 cm^{-1} specular reflectance spectra of nontronite (NAu-1) calcined at various temperatures. (b) The 100–1400 cm^{-1} specular reflectance spectra of nontronite (NAu-2) calcined at various temperatures. Linear vertical offset is applied to the spectra for clarity.

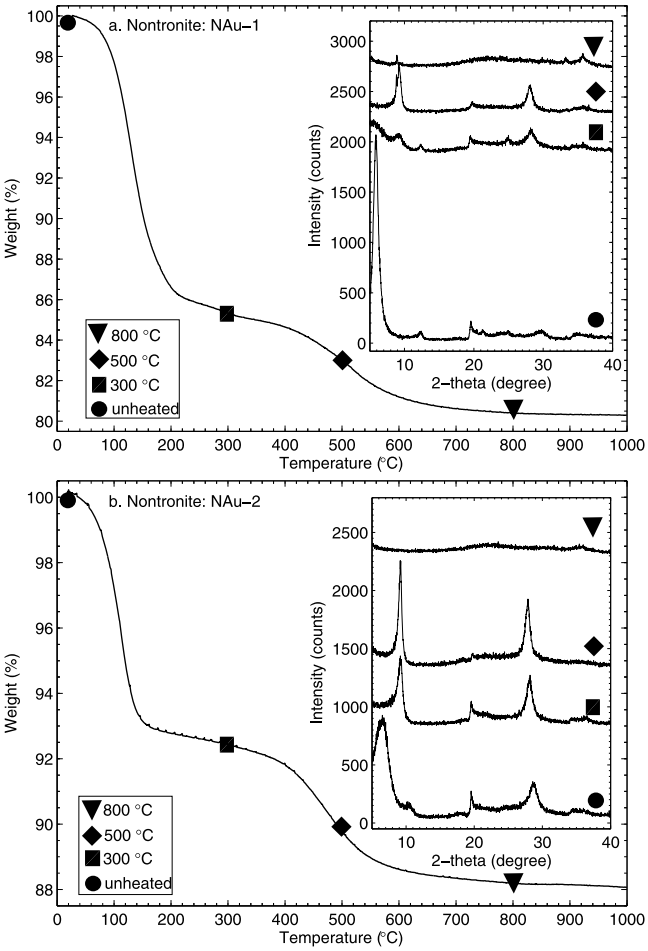

Figure 12. TGA plots and X-ray diffraction profiles (offset) of (a) NAu-1 nontronite and (b) NAu-2 nontronite.

(Figure 13a), but OH libration bands near 600–800 cm^{-1} [*Farmer*, 1974] remained as broad and weak features at 500°C and were absent in the 800°C ATR spectrum. The 943 cm^{-1} Si-O stretching band became very broad at 500°C and shifts to lower wave numbers at temperatures > 700°C. The Si-O bending vibration bands at ~400 cm^{-1} also changed distinctly when clinochlore was heated to 500°C.

4.3.2. Specular Reflectance Spectra

[58] The Si-O stretching bands near 950–1100 cm^{-1} disappeared at 500°C and a new broad band at ~1084 cm^{-1} formed (Figure 13b). The multiple Si-O bending bands near 400–550 cm^{-1} combined together to form a single band around 475 cm^{-1} after heating to 500°C. Bands at 650–800 cm^{-1} which were due to OH librations and a strong reflectance feature around 380 cm^{-1} all became very weak upon heating to 500°C. After 800°C heating, all spectral features formed at lower temperatures disappeared, and spectra of 800 and 900°C clinochlore were dominated by a peak at ~900 cm^{-1} and complex multiple peaks near 200–450 cm^{-1}.

4.3.3. Thermogravimetric and X-Ray Diffraction Analysis

[59] The TGA curve for clinochlore showed a weight loss from ~550°C to 800°C, immediately followed by a second, more abrupt weight loss from ~800°C to 900°C (Figure 13c). Previous studies [e.g., *Villieras et al.*, 1994] concluded that the first TGA weight loss was due to the dehydroxylation of the interlayer "brucite" sheets, and the loss of OH groups from the 2:1 layers produced the second weight loss. Changes in the XRD patterns as a function of heating were consistent with TGA results. The 001 reflection increased in intensity at 500°C and the other 00*l* reflections generally decreased in intensity. Clinochlore lost its original structure at 700°C and at 900°C the sample transformed to new phases.

4.4. Sepiolite-Palygorskite Group

4.4.1. Attenuated Total Reflectance Spectra

[60] In the case of palygorskite (PFl-1), the disappearance of the structural OH-stretching bands at 3539 cm^{-1} and 3616 cm^{-1} and the 912 cm^{-1} Al-Al-OH deformation band [*Madejová and Komadel*, 2001] at 400°C indicates that most of the hydroxyl groups have been removed from the palygorskite structure (Figure 14a). The H_2O bending band around ~1650 cm^{-1} shifted to ~1620 cm^{-1} at 100°C and then maintained its position until 600°C. However, the 1620 cm^{-1} feature was very weak above 400°C. The Si-O stretching band at 976 cm^{-1} shifted to 1018 cm^{-1} above 400°C and was at ~1051 cm^{-1} at 900°C. The peak around 800 cm^{-1} was assigned to the Si-O stretching band of quartz [*Madejová and Komadel*, 2001] and existed throughout the heating process. In addition, two spectral features existed only in certain temperature ranges: the ~870 cm^{-1} absorption band was present from 400°C to 600°C and the ~940 cm^{-1} band appeared after palygorskite is heated to 800°C.

[61] The spectral changes of sepiolite (SepSp-1) due to heating can be divided into four steps (Figure 14b): (1) no significant change was observed until 200°C; (2) at 300°C, the H_2O bending band at ~1660 cm^{-1} and Si-O stretching band around 1210 cm^{-1} disappeared and another Si-O stretching band at ~972 cm^{-1} shifted toward lower frequency (~940 cm^{-1}); (3) at 400°C, two peaks around 3620 cm^{-1} and 3560 cm^{-1} attributed to OH stretching disappeared, along with the 1620 cm^{-1} H_2O bending band. Correspondingly, the spectral features around 1000 cm^{-1} which were due to Si-O stretching vibrations became distinctly different from original spectral features; (4) the OH deformation and translation bands throughout the 600–800 cm^{-1} region [*Frost et al.*, 2001] disappeared at 800°C, consistent with the disappearance of the 3690 cm^{-1} OH-stretching band at the same temperature. The Si-O stretching bands around 1000 cm^{-1} changed significantly after 800°C heating and were replaced by multiple spectral features over the rang 900–1200 cm^{-1}.

4.4.2. Specular Reflectance Spectra

[62] For PFl-1 palygorskite, the Si-O stretching bands at ~1130 cm^{-1}, ~1040 cm^{-1}, and ~987 cm^{-1} combined at 400°C to form a new feature centered at ~1053 cm^{-1}. This new band began to shift toward high wave numbers and ended near 1107 cm^{-1} at 900°C (Figure 15a). The weak 910 cm^{-1} OH-deformation band disappeared at 400°C. A new spectral band was formed at ~870 cm^{-1} upon heating to 400°C and disappeared at 700°C. Beginning at 300°C, PFl-1 palygorskite began to lose its Si-O bending bands near ~400–550 cm^{-1}, and this spectral range was dominated by a single peak at ~460 cm^{-1} up to 800°C.

[63] In the case of SepSp-1 sepiolite, with increasing temperature, significant spectral changes in the Si-O stretching region around 1000 cm^{-1} and in the Si-O bending region

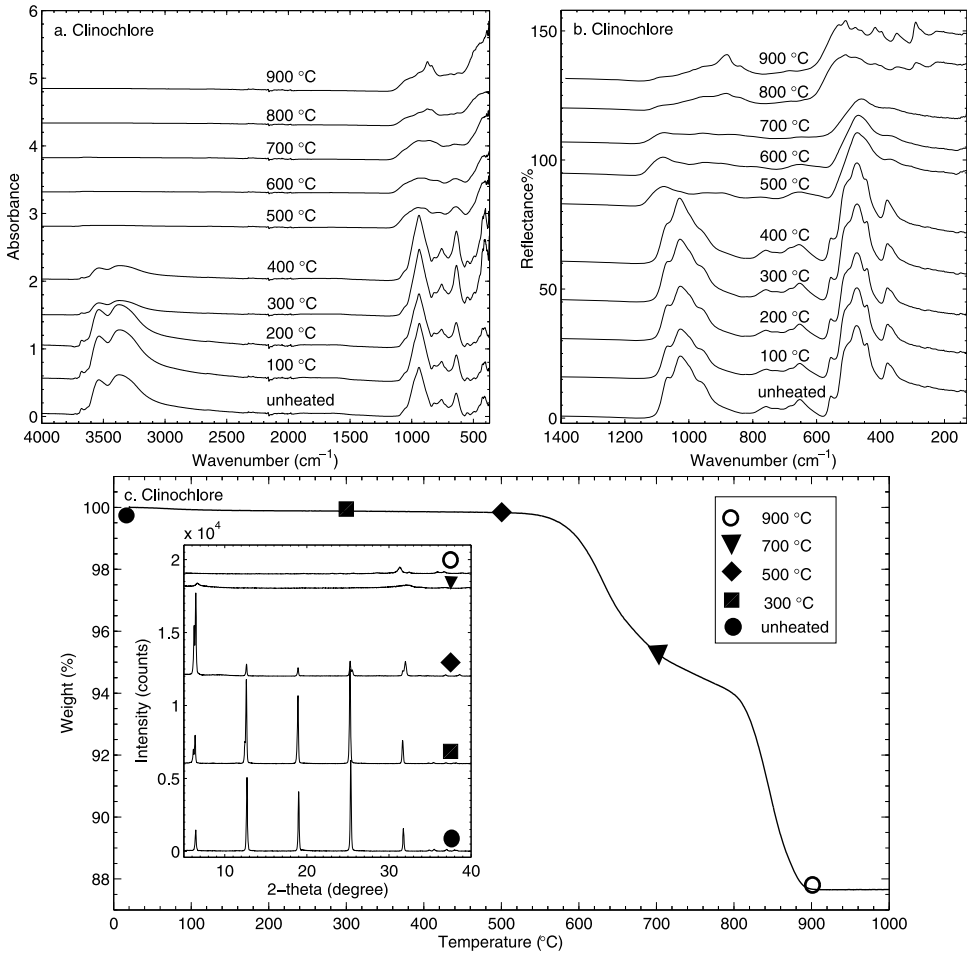

Figure 13. (a) The 370–4000 cm^{-1} ATR spectra of clinochlore calcined at various temperatures. (b) The 130–1400 cm^{-1} specular reflectance spectra of clinochlore calcined at various temperatures. Linear vertical offset is applied to the spectra for clarity. (c) TGA plots and X-ray diffraction profiles (offset) clinochlore.

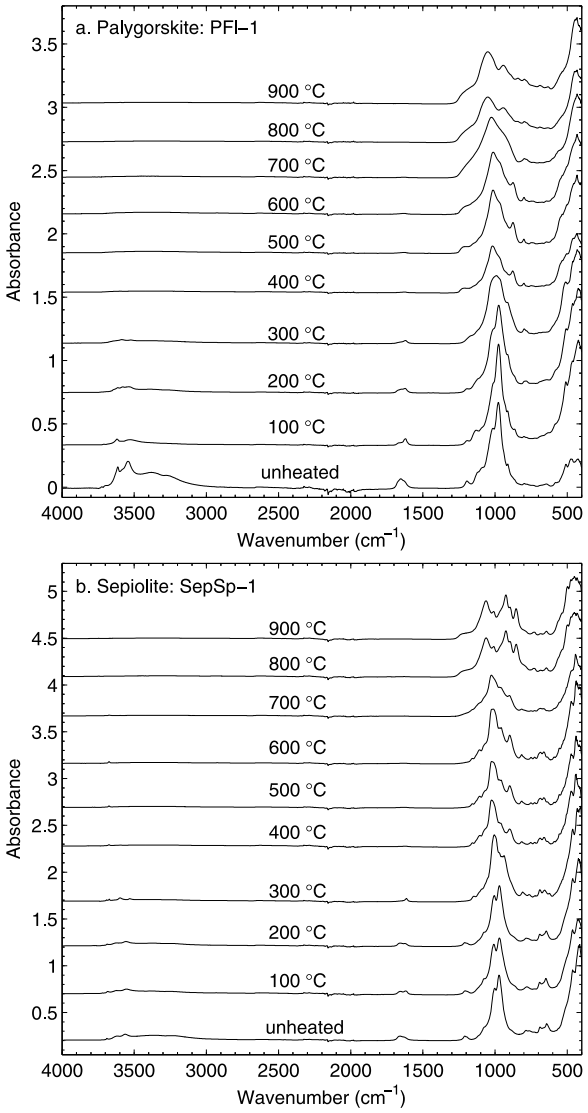

Figure 14. (a) The 400–4000 cm^{-1} ATR spectra of palygorskite (PFl-1) calcined at various temperatures. (b) The 400–4000 cm^{-1} ATR spectra of sepiolite (SepSp-1) calcined at various temperatures. Linear vertical offset is applied to the spectra for clarity.

near ~500 cm^{-1} took place at ~300°C, and then again around 800°C (Figure 15b). The OH-deformation band at ~970 cm^{-1} became very weak after 300°C heating and disappeared at 800°C. The OH translation bands in the 600–700 cm^{-1} range also disappeared at 800°C. The spectral features for SepSp-1 sepiolite observed after heating to 800°C, were completely different from those observed at lower temperatures. The spectra were no longer dominated by bands in two major spectral regions due to Si-O stretching (centered at ~1050 cm^{-1}) and Si-O bending (near ~400–550 cm^{-1}) and instead contained multiple bands near ~800–1200 cm^{-1}, a number of bands ~500 cm^{-1}, and several minor spectral features in the 200–400 cm^{-1} range.

4.4.3. Thermogravimetric and X-Ray Diffraction Analysis

[64] Both PFl-1 palygorskite and SepSp-1 sepiolite exhibited complex dehydration and dehydroxylation processes in their TGA curves (Figures 16a and 16b). Palygorskite lost weight in multiple steps, below ~150°C, from ~150°C to ~280°C, and from ~280°C to 500°C. Sepiolite showed even more complex weight loss behavior than palygorskite, with four overlapping events at ~150°C, from 150°C to 350°C, from 350°C to 550°C, and from 550°C to 850°C. The high temperature phases of palygorskite and sepiolite have been described in many previous studies [e.g., *Kulbicki*, 1959], which showed that both palygorskite and sepiolite transform to enstatite upon heating to 800°C or elevated temperatures. In this study, the formation of enstatite was apparent in the 800°C XRD pattern of sepiolite because main reflections of enstatite (610) (31°, 2θ) and (420) (28°, 2θ) were recorded, while no clear evidence in the 800°C XRD pattern of palygorskite showed the development of enstatite structure.

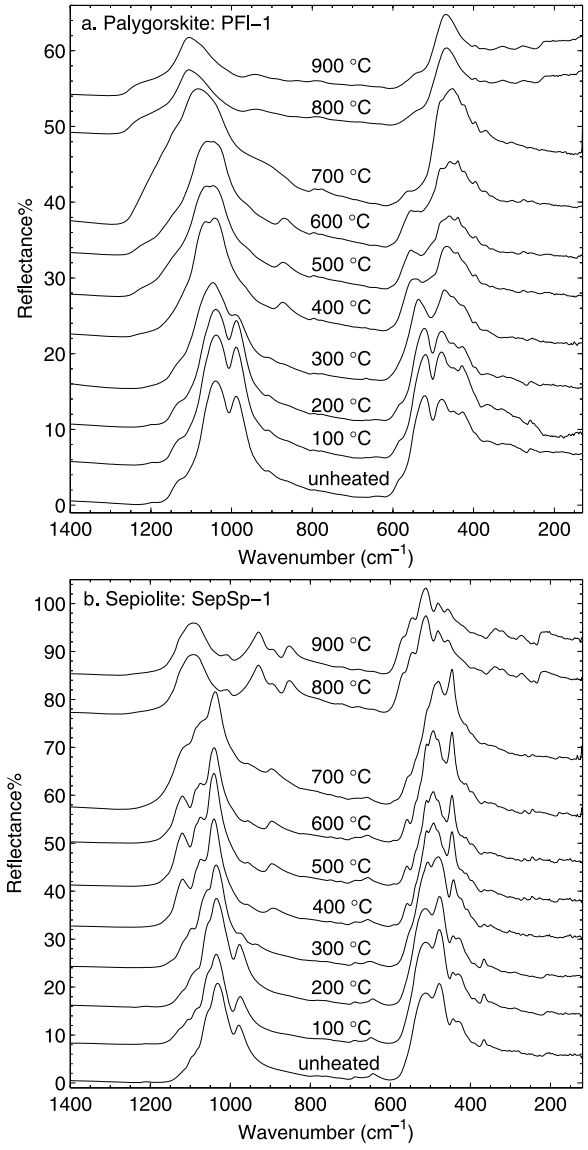

Figure 15. (a) The 130–1500 cm^{-1} specular reflectance spectra of palygorskite (PFl-1) calcined at various temperatures. (b) The 120–1400 cm^{-1} specular reflectance spectra of sepiolite (SepSp-1) calcined at various temperatures. Linear vertical offset is applied to the spectra for clarity.

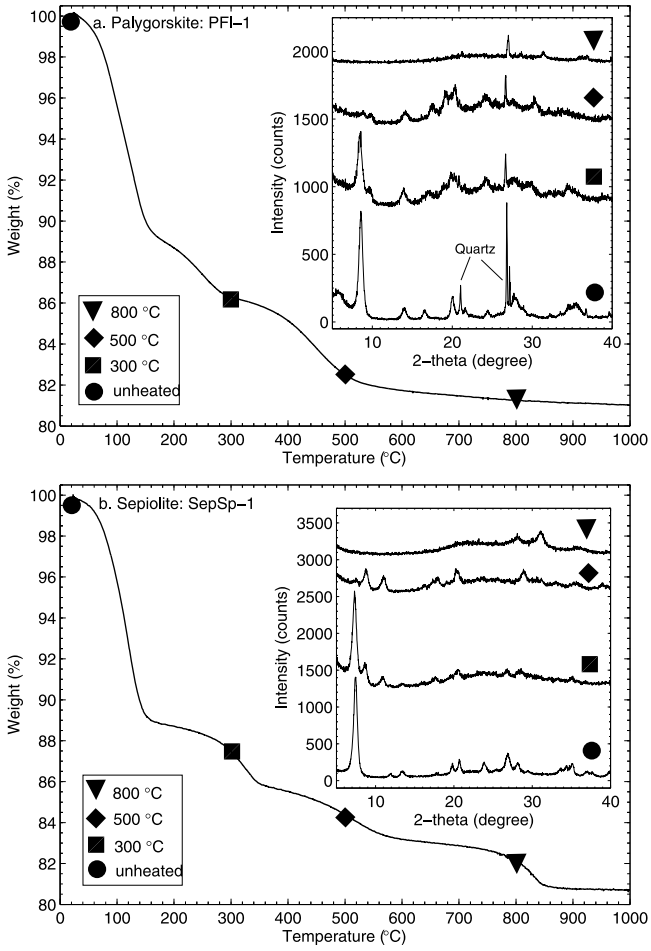

Figure 16. TGA plots and X-ray diffraction profiles (offset) of (a) PFl-1 palygorskite and (b) SepSp-1 sepiolite.

4.5. Zeolite Group

4.5.1. Attenuated Total Reflectance Spectra

[65] The infrared spectra of zeolites were summarized by *Breck* [1974b]. 27031 clinoptilolite lost its H_2O bending (~1630 cm^{-1}) feature at 800°C (Figure 17a). The spectral feature at ~1000 cm^{-1} due to tetrahedron asymmetric stretching mode showed no obvious change upon heating, although the band became weaker and broader at 800°C. The 790 cm^{-1} peak was assigned to the stretching modes involving mainly the tetrahedral atoms and remained until 900°C. The bands at ~500–650 cm^{-1} related to the double rings in the framework structures and the internal tetrahedral symmetric stretching bands over the range ~650–720 cm^{-1} all disappeared at 800°C.

[66] The spectral behavior of 27133 mordenite (Figure 17b) was similar to that of 27031 clinoptilolite upon heating. However, the OH-stretching bands near 3400 cm^{-1} and the H_2O bending band at ~1630 cm^{-1} persisted to 800°C, although they were very weak at higher temperatures.

4.5.2. Specular Reflectance Spectra

[67] The tetrahedral stretching band (~1086 cm^{-1}) of clinoptilolite showed no change until 700°C, and it shifted slightly to higher wave numbers (~1100 cm^{-1}) at 800°C (Figure 18a). Also a weak shoulder band at ~1200 cm^{-1} developed at 800°C. The weak band at ~780 cm^{-1} associated with symmetric stretching of external linkages persisted to 900°C. The ~600 cm^{-1} double-ring band disappeared at 800°C. The Si (Al)-O bending band at~470 cm^{-1} remained to 900°C. The weak shoulder band at ~378 cm^{-1}, related to the motion of the tetrahedral rings which form the pore openings in the zeolites [*Breck*, 1974b] disappeared at 700°C.

[68] The two adjacent tetrahedron stretching bands around 1050 cm^{-1} (Figure 18b) combined at 500°C and this new band shifted to 1100 cm^{-1} at 700°C. Two weak spectral features at ~550 and ~625 cm^{-1} appeared upon heating to 700°C and disappeared at 900°C. Other than these, the 1250 cm^{-1} Si (Al)-O stretching band, the 770 cm^{-1} stretching band of external linkages, and the 470 cm^{-1} Si (Al)-O bending band were remained to 900°C. No spectral features were observed in the far-IR range for mordenite.

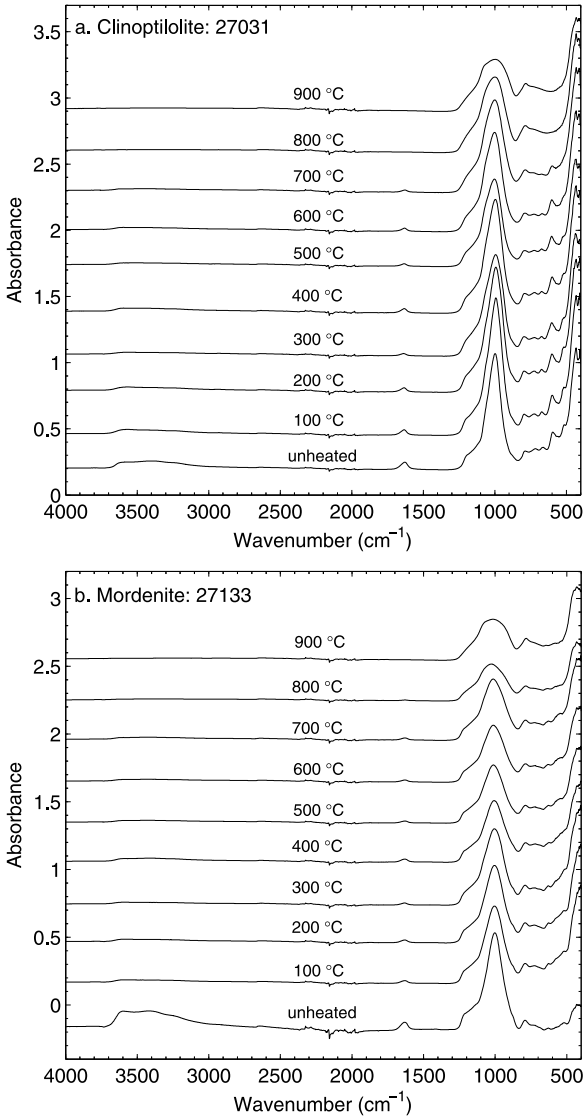

Figure 17. (a) The 400–4000 cm^{-1} ATR spectra of clinoptilolite (27031) calcined at various temperatures. (b) The 400–4000 cm^{-1} ATR spectra of mordenite (27133) calcined at various temperatures. Linear vertical offset is applied to the spectra for clarity.

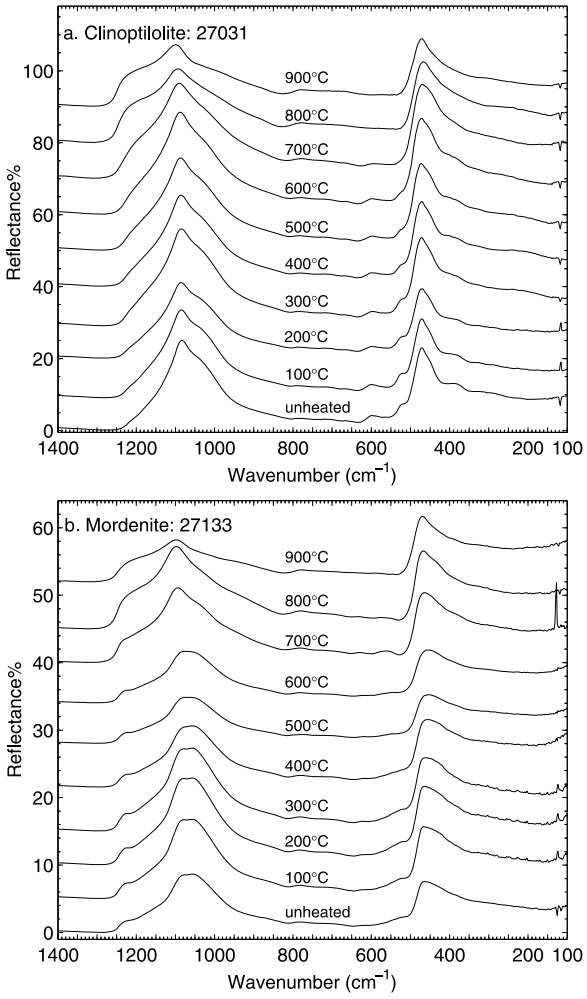

Figure 18. (a) The 100–1400 cm^{-1} specular reflectance spectra of clinoptilolite (27031) calcined at various temperatures. (b) The 100–1400 cm^{-1} specular reflectance spectra of mordenite (27133) calcined at various temperatures. Linear vertical offset is applied to the spectra for clarity.

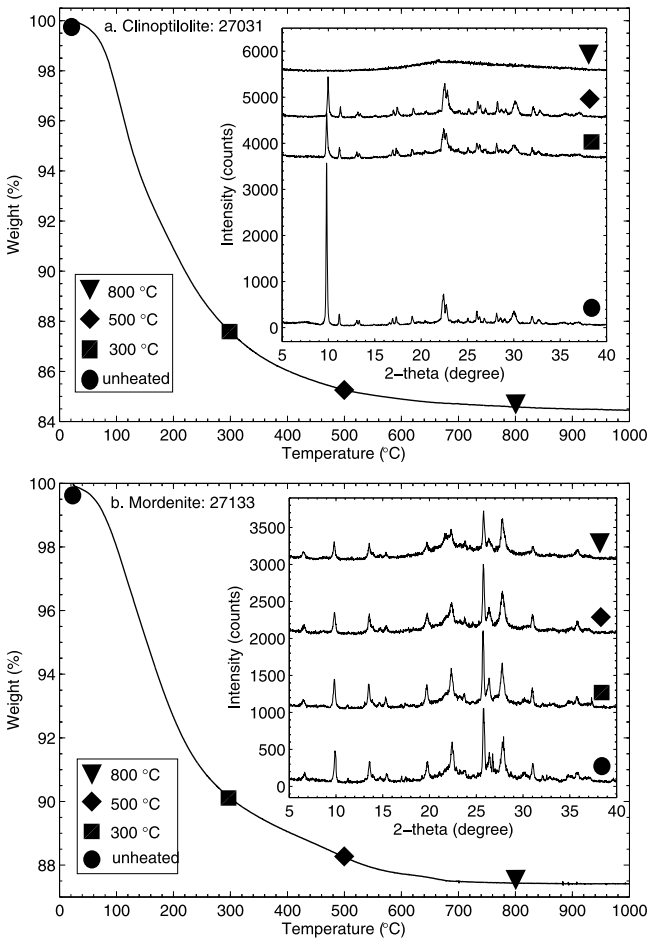

Figure 19. TGA plots and X-ray diffraction profiles (offset) of (a) 27031 clinoptilolite and (b) 27133 mordenite.

4.5.3. Thermogravimetric and X-Ray Diffraction Analysis

[69] TGA data for clinoptilolite and mordenite show a slow and continuous loss in weight throughout the heat treatments (Figures 19a and 19b), showing that these two natural zeolites release H_2O from their rigid cage structures gradually upon heating. The XRD results show that the mordenite structure is not affected significantly by 800°C heating whereas clinoptilolite transformed to an amorphous phase at 800°C.

5. Discussion

5.1. Effect of Adsorbed H_2O

[70] For most phyllosilicates analyzed here, TGA result showed that H_2O loss occurred at a low temperature (<200°–300°C), while ATR spectra revealed a much higher temperature (>400°–500°C) for the disappearance of the ~1630 cm^{-1} H_2O bending band. For example, the H_2O molecules of SCa-3 montmorillonite were lost by 200°C based on its TGA result (Figure 4b) whereas the H-O-H bending band of this montmorillonite was observed from its ATR spectrum up to 500°C (Figure 2b). This conflict is very likely due to the readsorption of water onto the sample because, during ATR measurements, the sample was exposed to open air for 5 min and phyllosilicates have extremely high specific surface area [e.g., *Dogan et al.*, 2006]. Therefore the evolution of the ~1630 cm^{-1} hydration band in ATR spectrum shows the change of the specific surface area due to heating treatment rather than the dehydration processes of phyllosilicates.

5.2. Effect of Octahedral Cations

[71] The concentration of Al^{3+} or Fe^{3+} in dioctahedral smectites may affect their spectral behaviors on heating. Syn-1 mica-montmorillonite and SBCa-1 beidellite contain the highest concentrations of Al^{3+} (36.75% and 30.71% Al_2O_3, respectively) in octahedral sites, and their IR spectra, particularly the multiple bands in the Si-O bending regions, did not show significant change until 800°C. The montmorillonite series includes four samples in this study: SWy-2 (20.12% Al_2O_3), STx-1 (16.17% Al_2O_3), SAz-1 (17.20% Al_2O_3), and SCa-3 (12.47% Al_2O_3). The first distinct spectral change upon heating occurred around 600°C for SWy-2, whereas the spectra of the three other montmorillonites changed significantly around 500°C. NAu-1 and NAu-2 nontronites are both Fe^{3+} rich smectites, and they lost their original spectral features completely at 400°C. According to the above observations, Al-rich smectites may have greater thermal stability and maintain their spectral features to higher temperatures than Fe-rich smectites, which was also shown by previous investigators *Gavin and Chevrier* [2010].

[72] Mg phyllosilicates tend to transform to an enstatite phase at ~800°C [e.g., *Kulbicki*, 1959]. The 800°C IR spectral features of the trioctahedral phyllosilicates hectorite, saponite, and sepiolite were completely different from the original spectral features that were dominated by Si-O stretching and Si-O bending bands, indicating the formation of a new phase, likely an enstatite structure. It was also observed that high-Mg phyllosilicates clinochlore (23.56% MgO) and palygorskite (9.52% MgO), moderate-Mg smectites SAz-1 (5.80% MgO) and SCa-3 (8.55% MgO) montmorillonites, and even low-Mg STx-1 (3.43% MgO) montmorillonite all developed new IR spectral features around 900 cm^{-1} when at 800°C. No similar new spectral features were observed for SWy-2 (2.68% MgO) montmorillonite at 800°C.

6. Summary and Conclusions

[73] This study documents the effects of heating phyllosilicates and zeolite minerals based on ATR, IR reflectance, TGA, and powder XRD measurements. Heat treatment produces distinct changes in the infrared spectral features (~100–4000 cm^{-1}) of phyllosillicates and zeolites. These changes are associated with dehydration and/or dehydroxylation processes, determined primarily by the specific crystal structures and affected by their octahedral and extraframework cation compositions:

[74] 1. For phyllosilicate samples, the OH stretching (~3600 cm^{-1}), OH bending (~590–950 cm^{-1}), and/or H_2O bending (~1630 cm^{-1}) bands all become very weak or completely disappear upon heating to temperatures > 500°C. The spectral changes associated with SiO_4 vibrations (~1000 cm^{-1} and ~500 cm^{-1}) show large variations depending on the compositions and structures of phyllosilicates. Spectral features of kaolinite change significantly at ~400°C and the new bands are relatively stable until 900°C. Most smectite samples display two distinct spectral changes with increased temperature, which may be related to their dehydration and dehydroxylation processes, respectively. Clinochlore also exhibited dual changes in spectral features on heating, likely due to the presence of two different types of hydroxyl groups. The modulated tetrahedral sheets of palygorskite/sepiolite minerals showed more complex spectral changes on heating than other phyllosilicates included in this study. Compared to the phyllosilicates, the spectral features of two natural zeolites, clinoptilolite and mordenite, are less affected by thermal treatments. Even after heating to 900°C, the IR spectral features do not show significant differences from those of unheated zeolites. These spectral results are consistent with the fact that the three-dimensionally rigid crystal structure of zeolite is stabler than the layer structure of phyllosilicates.

[75] 2. The composition of octahedral sites showed a great influence on spectral behaviors of phyllosilicates: IR spectra of Al^{3+} rich smectites are stabler than those of Fe^{3+} rich smectites; spectral behaviors of Mg^{2+} rich phyllosilicates are distinctly affected by the formation of new crystal phases around 700°C; phyllosilicates with a small amount of Mg^{2+} on their octahedral sites all showed new spectral band at ~900 cm^{-1} upon heating to 700°C or higher temperatures.

[76] **Acknowledgments.** This manuscript was greatly improved by the careful work of Editor Robert Carlson, and thorough reviews from Patricia Gavin and an anonymous reviewer, for which we are very grateful. We are also grateful for support from Mars Fundamental Research Program NNX08AN62G.

References

Abramov, O., and D. A. Kring (2005), Impact-induced hydrothermal activity on early Mars, *J. Geophys. Res.*, *110*, E12S09, doi:10.1029/2005JE002453.

Aceman, S., N. Lahav, and S. Yariv (1997), XRD study of the dehydration and rehydration of Al-pillared smectites differing in source of charge, *J. Therm. Anal.*, *50*, 241–256, doi:10.1007/BF01979565.

Armbruster, T., and M. E. Gunter (2001), Crystal structure of natural zeolites, in *Natural Zeolites: Occurrence, Properties, Application*, *Rev.*

Mineral. Geochem., vol. 45, edited by D. L. Bish and D. W. Ming, pp. 1–57, Mineral. Soc. of Am., Washington, D. C.

Bailey, S. W. (1980), Structures of layer silicates, in *Crystal Structures of Clay Minerals and Their X-Ray Identification*, edited by G. W. Brindley and G. Brown, pp. 1–124, Mineral. Soc., London.

Ballet, O., J. M. D. Coey, and K. J. Burke (1985), Magnetic properties of sheet silicates; 2:1:1 layer minerals, *Phys. Chem. Miner.*, *12*, 370–378, doi:10.1007/BF00654348.

Bandfield, J. L. (2002), Global minerals distributions on Mars, *J. Geophys. Res.*, *107*(E6), 5042, doi:10.1029/2001JE001510.

Bandfield, J. L., V. E. Hamilton, and P. R. Christensen (2000), A global view of Martian surface compositions from MGS-TES, *Science*, *287*, 1626–1630, doi:10.1126/science.287.5458.1626.

Barrer, R. M. (1978), Zeolite frameworks, cations and water molecules, in *Zeolites and Clay Minerals as Sorbents and Molecular Sieves*, pp. 32–102, Academic, London.

Barrer, R. M. (1982), Occurrence, classification and some properties of zeolites, in *Hydrothermal Chemistry of Zeolites*, pp. 1–42, Academic, London.

Bibring, J.-P., et al. (2005), Mars surface diversity as revealed by the OMEGA/Mars Express observations, *Science*, *307*, 1576–1581, doi:10.1126/science.1108806.

Bibring, J.-P., et al. (2006), Global mineralogical and aqueous Mars history derived from OMEGA/Mars Express data, *Science*, *312*, 400–404, doi:10.1126/science.1122659.

Bish, D. L. (1984), Effects of exchangeable cation composition on the thermal expansion/contraction of clinoptilolite, *Clays Clay Miner.*, *32*(6), 444–452, doi:10.1346/CCMN.1984.0320602.

Bish, D. L. (1988), Effects of composition on the dehydration behavior of clinoptilolite and heulandite, in *Occurrence, Properties and Utilization of Natural Zeolites*, edited by D. Kallo and H. S. Sherry, 565 pp., Akadémiai Kiadó, Budapest.

Bish, D. L., and J. W. Carey (2001), Thermal properties of natural zeolites, in *Natural Zeolites: Occurrence, Properties, Applications*, edited by D. L. Bish and D. W. Ming, 403 pp., Mineral. Soc. of Am., Washington, D. C.

Bish, D. L., J. W. Carey, D. T. Vaniman, and S. J. Chipera (2003), Stability of hydrous minerals on the Martian surface, *Icarus*, *164*, 96–103, doi:10.1016/S0019-1035(03)00140-4.

Bishop, J. L., et al. (2008a), Phyllosilicate diversity and past aqueous activity revealed at Mawrth Vallis, Mars, *Science*, *321*, 830–833, doi:10.1126/science.1159699.

Bishop, J. L., M. D. Lane, M. D. Dyar, and A. J. Brown (2008b), Reflectance and emission spectroscopy study of four groups of phyllosilicates: Smectites, kaolinite-serpentines, chlorites and micas, *Clay Miner.*, *43*, 35–54, doi:10.1180/claymin.2008.043.1.03.

Bishop, J. L., N. K. McKeown, D. J. DesMarais, E. Z. Noe Dobrea, M. Parente, F. Seelos, S. L. Murchie, and J. F. Mustard (2009), The ancient phyllosilicates at Mawrth Vallis and what they can tell us about possible habitable environments on early Mars, *Proc. Lunar Planet. Sci. Conf.*, *40th*, 2239.

Boslough, M. B., R. J. Weldon, and T. J. Ahrens (1980), Impact-induced water loss from serpentine, nontronite and kernite, *Proc. Lunar Planet. Sci. Conf.*, *11th*, 2145–2158.

Breck, D. W. (1974a), Structure of zeolites, in *Zeolite Molecular Sieves: Structure, Chemistry, and Use*, pp. 29–185, John Wiley, London.

Breck, D. W. (1974b), Chemical properties and reactions of zeolites, in *Zeolite Molecular Sieves: Structure, Chemistry, and Use*, pp. 441–528, John Wiley, London.

Bruckenthal, E. A., and R. B. Singer (1987), Spectral effects of dehydration on phyllosilicates, *Proc. Lunar Planet. Sci. Conf.*, *18th*, 135.

Carroll, D. L., T. F. Kemp, T. J. Bastow, and M. E. Smith (2005), Solid-state NMR characterisation of the thermal transformation of a Hungarian white illite, *Solid State Nucl. Magn. Reson.*, *28*, 31–43, doi:10.1016/j.ssnmr.2005.04.001.

Che, C., and T. D. Glotch (2010), The effect of high temperatures on the emission and VNIR reflectance spectra of phyllosilicates and zeolites, *Proc. Lunar Planet. Sci. Conf.*, *41st*, 1513.

Chemtob, S. M., and T. D. Glotch (2007), Linear deconvolution of attenuated total reflectance infrared spectra of fine-grained mineral mixtures, *Proc. Lunar Planet. Sci. Conf.*, *38th*, 1097.

Cruciani, G. (2006), Zeolites upon heating: Factors governing their thermal stability and structural changes, *J. Phys. Chem. Solids*, *67*, 1973–1994, doi:10.1016/j.jpcs.2006.05.057.

Dogan, A. U., M. Dogan, M. Onal, Y. Sarikaya, A. Aburub, and D. E. Wurster (2006), Baseline studies of the Clay Minerals Society source clays: Specific surface area by the Brunauer Emmett Teller (BET) method, *Clays Clay Miner.*, *54*, 62–66, doi:10.1346/CCMN.2006.0540108.

Drachman, S. R., G. E. Roch, and M. E. Smith (1997), Solid state NMR characterisation of the thermal transformation of Fuller's Earth, *Solid State Nucl. Magn. Reson.*, *9*, 257–267, doi:10.1016/S0926-2040(97)00069-6.

Ehlmann, B. L., et al. (2009), Identification of hydrated silicate minerals on Mars using MRO-CRISM: Geologic context near Nili Fossae and implications for aqueous alteration, *J. Geophys. Res.*, *114*, E00D08, doi:10.1029/2009JE003339.

Fairén, A. G., et al. (2010), Noachian and more recent phyllosilicates in impact craters on Mars, *Proc. Natl. Acad. Sci. U. S. A.*, *107*, 12,095–12,100, doi:10.1073/pnas.1002889107.

Farmer, V. C. (1974), The layer silicates, in *The Infrared Spectra of Minerals*, edited by V. C. Farmer, pp. 331–363, Mineral. Soc., London.

Farrand, W. H., T. D. Glotch, J. W. Rice Jr., J. A. Hurowitz, and G. A. Swayze (2009), Discovery of jarosite within the Mawrth Vallis region of Mars: Implications for the geologic history of the region, *Icarus*, *204*, 478–488, doi:10.1016/j.icarus.2009.07.014.

Fitzgerald, J. J., S. F. Dec, and A. I. Hamza (1989), Observation of 5-coordinated Al in pyrophyllite dehydroxylate by solid-state ^{27}Al NMR spectroscopy at 14 T, *Am. Mineral.*, *74*, 1405–1408.

Fitzgerald, J. J., A. I. Hamza, S. F. Dec, and C. E. Bronnimann (1996), Solid-state ^{27}Al and ^{29}Si NMR and ^{1}H CRAMPS studies of the thermal transformations of the 2:1 phyllosilicate pyrophyllite, *J. Phys. Chem.*, *100*, 17,351–17,360, doi:10.1021/jp961499f.

Frost, R. L., and P. F. Barron (1984), Solid-state silicon-29 and aluminum-27 nuclear magnetic resonance investigation of the dehydroxylation of pyrophyllite, *J. Phys. Chem.*, *88*, 6206–6209, doi:10.1021/j150669a030.

Frost, R. L., and J. T. Kloprogge (2000), Vibrational spectroscopy of ferruginous smectite and nontronite, *Spectrochim. Acta, Part A*, *56*, 2177–2189, doi:10.1016/S1386-1425(00)00279-1.

Frost, R. L., O. B. Locos, H. Ruan, and J. T. Kloprogge (2001), Near-infrared and mid-infrared spectroscopic study of sepiolites and palygorskites, *Vib. Spectrosc.*, *27*, 1–13, doi:10.1016/S0924-2031(01)00110-2.

Frost, R. L., J. T. Kloprogge, and D. Zhe (2002), The Garfield and Uley nontronites-an infrared spectroscopic comparison, *Spectrochim. Acta, Part A*, *58*, 1881–1894, doi:10.1016/S1386-1425(01)00638-2.

Gavin, P., and V. Chevrier (2010), Thermal alteration of nontronite and montmorillonite: Implications for the Martian surface, *Icarus*, *208*, 721–734, doi:10.1016/j.icarus.2010.02.027.

Gavin, P., V. Chevrier, and K. Ninagawa (2008), Effect of impact and heating on the spectral properties of clays on Mars, *Proc. Lunar Planet. Sci. Conf.*, *39th*, 2033.

Green, J. M., K. J. D. Mackenzie, and J. H. Sharp (1970), Thermal reactions of synthetic hectorite, *Clays Clay Miner.*, *18*, 339–346, doi:10.1346/CCMN.1970.0180606.

Grim, R. E., and G. Kulbicki (1961), Montmorillonite: High temperature reactions and classification, *Am. Mineral.*, *46*, 1329–1369.

Guggenheim, S., and A. F. Koster van Groos (2001), Baseline studies of the clay minerals society source clays: Thermal analysis, *Clays Clay Miner.*, *49*, 433–443, doi:10.1346/CCMN.2001.0490509.

Harris, W. G., K. A. Hollien, S. R. Bates, and W. A. Acree (1992), Dehydration of hydroxyl-interlayered vermiculite as a function of time and temperature, *Clays Clay Miner.*, *40*, 335–340, doi:10.1346/CCMN.1992.0400314.

He, H. P., J. G. Guo, J. X. Zhu, and C. Hu (2003), ^{29}Si and ^{27}Al MAS NMR study of the thermal transformations of kaolinite from North China, *Clay Miner.*, *38*, 551–559, doi:10.1180/0009855033840114.

Keeling, J. L., M. D. Raven, and W. P. Gates (2000), Geology and characterization of two hydrothermal nontronites from weathered metamorphic rocks at the Uley graphite mine, South Australia, *Clays Clay Miner.*, *48*, 537–548, doi:10.1346/CCMN.2000.0480506.

Kloprogge, J. T., and R. L. Frost (2005), Infrared emission spectroscopy of clay minerals, in *The Application of Vibrational Spectroscopy to Clay Minerals and Layered Double Hydroxides*, *CMS Workshop Lectures*, vol. 13, edited by J. T. Kloprogge, pp. 99–124, Clay Mineral Soc., Aurora, Colo.

Kloprogge, J. T., S. Komarneni, K. Yanagisawa, R. L. Frost, and R. Fry (1998), Infrared study of some synthetic and natural beidellites, *J. Mater. Sci. Lett.*, *17*, 1853–1855, doi:10.1023/A:1006694629015.

Kloprogge, J. T., R. L. Frost, and L. Hickey (1999a), Infrared absorption and emission study of synthetic mica-montmorillonite in comparison to rectorite, beidellite and paragonite, *J. Mater. Sci. Lett.*, *18*, 1921–1923, doi:10.1023/A:1006672913161.

Kloprogge, J. T., R. Fry, and R. L. Frost (1999b), An infrared emission spectroscopic study of the thermal transformation mechanims in Al_{13}-pillared clay catalysts with and without tetrahedral substitutions, *J. Catal.*, *184*, 157–171, doi:10.1006/jcat.1999.2444.

Kloprogge, J. T., R. L. Frost, and L. Hickey (2000), Infrared emission spectroscopic study of the dehydroxylation of some hectorites, *Thermochim. Acta*, *345*, 145–156, doi:10.1016/S0040-6031(99)00359-7.

Kulbicki, G. (1959), High temperature phases in sepiolite, attapulgite and saponite, *Am. Mineral.*, *44*, 752–764.

Lambert, J. F., W. S. Millman, and J. J. Fripiat (1989), Revisiting kaolinite dehydroxylation: A ^{29}Si and ^{27}Al MAS NMR study, *J. Am. Chem. Soc.*, *111*, 3517–3522, doi:10.1021/ja00192a005.

Lange, M. A., and T. J. Ahrens (1982), Impact induced dehydration of serpentine and the evolution of planetary atmosphere, *Proc. Lunar Planet. Sci. Conf.*, *13th*, A451–A456.

Loizeau, D., et al. (2007), Phyllosilicates in the Mawrth Vallis region of Mars, *J. Geophys. Res.*, *112*, E08S08, doi:10.1029/2006JE002877.

Madejová, J., and P. Komadel (2001), Baseline studies of the clay minerals society source clays: Infrared methods, *Clays Clay Miner.*, *49*, 410–432, doi:10.1346/CCMN.2001.0490508.

Mangold, N., et al. (2007), Mineralogy of the Nili Fossae region with OMEGA/Mars Express data: 2. Aqueous alteration of the crust, *J. Geophys. Res.*, *112*, E08S04, doi:10.1029/2006JE002835.

Massiot, D., P. Dion, J. F. Alcover, and F. Bergaya (1995), ^{27}Al and ^{29}Si MAS NMR study of kaolinite thermal decomposition by controlled rate thermal analysis, *J. Am. Ceram. Soc.*, *78*, 2940–2944, doi:10.1111/j.1151-2916.1995.tb09067.x.

McManus, J., S. E. Ashbrook, K. J. D. MacKenzie, and S. Wimperis (2001), ^{27}Al multiple-quantum MAS and ^{27}Al{^{1}H} CPMAS NMR study of amorphous aluminosilicates, *J. Non-Cryst. Solids*, *282*, 278–290, doi:10.1016/S0022-3093(01)00313-1.

Mermut, A. R., and A. Faz Cano (2001), Baseline studies of the clay minerals society source clays: Chemical analyses of major elements, *Clays Clay Miner.*, *49*, 381–386, doi:10.1346/CCMN.2001.0490504.

Michalski, J. R., and R. L. Fergason (2009), Composition and thermal inertia of the Mawrth Vallis region of Mars and THEMIS data, *Icarus*, *199*, 25–48, doi:10.1016/j.icarus.2008.08.016.

Michalski, J. R., and E. Z. Noe Dobrea (2007), Evidence for a sedimentary origin of clay minerals in the Mawrth Vallis region, Mars, *Geology*, *35*, 951–954, doi:10.1130/G23854A.1.

Michalski, J. R., M. D. Kraft, T. G. Sharp, L. B. Williams, and P. R. Christensen (2005), Mineralogical constraints on the high-silica Martian surface component observed by TES, *Icarus*, *174*, 161–177, doi:10.1016/j.icarus.2004.10.022.

Michalski, J. R., M. D. Kraft, T. G. Sharp, L. B. Williams, and P. R. Christensen (2006), Emission spectroscopy of clay minerals and evidence for poorly crystalline aluminosilicates on Mars from Thermal Emission Spectrometer data, *J. Geophys. Res.*, *111*, E03004, doi:10.1029/2005JE002438.

Michalski, J. R., F. Poulet, J.-P. Bibring, and N. Mangold (2010), Analysis of phyllosilicate deposits in Nili Fossae region of Mars: Comparison of TES and OMEGA data, *Icarus*, doi:10.1016/j.icarus.2009.09.006.

Milliken, R. E., and J. F. Mustard (2005), Quantifying absolute water content of minerals using near-infrared reflectance spectroscopy, *J. Geophys. Res.*, *110*, E12001, doi:10.1029/2005JE002534.

Milliken, R. E., J. F. Mustard, F. Poulet, D. Jouglet, J.-P. Bibring, B. Gondet, and Y. Langevin (2007), Hydration state of the Martian surface as seen by Mars Express OMEGA: 2. H_2O content of the surface, *J. Geophys. Res.*, *112*, E08S07, doi:10.1029/2006JE002853.

Moore, D. M., and R. C. Reynolds Jr. (1989a), Structure and properties of clay minerals, in *X-Ray Diffraction and the Identification and Analysis of Clay Minerals*, pp. 102–178, Oxford Univ. Press, Oxford, U. K.

Moore, D. M., and R. C. Reynolds Jr. (1989b), *X-Ray Diffraction and the Identification and Analysis of Clay Minerals*, pp. 187–190, Oxford Univ. Press, Oxford, U. K.

Murchie, S. L., et al. (2009), Compact Reconnaissance Imaging Spectrometer for Mars investigation and data set from the Mars Reconnaissance Orbiter's primary science phase, *J. Geophys. Res.*, *114*, E00D07, doi:10.1029/2009JE003344.

Mustard, J. F., et al. (2007), CRISM-OMEGA observations of phyllosilicate-olivine stratigraphy in Nili Fossae, Mars, *Proc. Lunar Planet. Sci. Conf.*, *38th*, 2071.

Mustard, J. F., et al. (2008), Hydrated silicate minerals on Mars observed by the Mars Reconnaissance Orbiter CRISM instrument, *Nature*, *454*, 305–309, doi:10.1038/nature07097.

Newsam, J. M. (1986), The zeolite cage structure, *Science*, *231*, 1093–1099, doi:10.1126/science.231.4742.1093.

Ohnishi, I., and K. Tomeoka (2002), Dark inclusions in the Mokoia CV3 chondrite: Evidence for aqueous alteration and subsequent thermal and shock metamorphism, *Met. Planet. Sci.*, *37*, 1843–1856, doi:10.1111/j.1945-5100.2002.tb01168.x.

Post, J. L. (1984), Saponite from near Ballarat, California, *Clays Clay Miner.*, *32*, 147–153, doi:10.1346/CCMN.1984.0320209.

Poulet, F., et al. (2005), Phyllosilicates on Mars and implications for early Martian climate, *Nature*, *438*, 623–627, doi:10.1038/nature04274.

Poulet, F., C. Gomez, J.-P. Bibring, Y. Langevin, B. Gondet, P. Pinet, G. Belluci, and J. Mustard (2007), Martian surface mineralogy from Observatoire pour la Minéralogie, l'Eau, les Glaces et l'Activité on board the Mars Express spacecraft (OMEGA/MEx): Global mineral maps, *J. Geophys. Res.*, *112*, E08S02, doi:10.1029/2006JE002840.

Prasad, P. S. R., and K. S. Prasad (2007), Dehydration and rehydration of mesolite: An *in situ* FTIR study, *Microporous Mesoporous Mater.*, *100*, 287–294, doi:10.1016/j.micromeso.2006.11.012.

Prasad, P. S. R., K. S. Prasad, and S. R. Murthy (2005), Dehydration of natural stilbite: An in situ FTIR study, *Am. Mineral.*, *90*, 1630–1640, doi:10.2138/am.2005.1747.

Pruett, R. J., and H. L. Webb (1993), Sampling and analysis of KGa-1b well-crystallized kaolin source clay, *Clays Clay Miner.*, *41*, 514–519, doi:10.1346/CCMN.1993.0410411.

Roch, G. E., M. E. Smith, and S. R. Drachman (1998), Solid state NMR characterization of the thermal transformation of an illite-rich clay, *Clays Clay Miner.*, *46*, 694–704, doi:10.1346/CCMN.1998.0460610.

Rocha, J. (1999), Single- and triple-quantum ^{27}Al MAS NMR study of the thermal transformation of kaolinite, *J. Phys. Chem. B*, *103*, 9801–9804, doi:10.1021/jp991516b.

Rocha, J., and J. Klinowski (1990), ^{29}Si and ^{27}Al magic-angle-spinning NMR studies of the thermal transformation of kaolinite, *Phys. Chem. Miner.*, *17*, 179–186, doi:10.1007/BF00199671.

Rodriguez-Fuentes, G., A. R. Ruiz-Salvador, M. Mir, O. Picazo, G. Quintana, and M. Delgado (1998), Thermal and cation influence on IR vibrations of modified natural clinoptilolite, *Microporous Mesoporous Mater.*, *20*, 269–281, doi:10.1016/S1387-1811(97)00013-9.

Ruff, S. W. (2003), Basaltic andesite or weathered basalt: A new assessment, *Proc. Int. Conf. Mars*, *6th*, 3258.

Ruff, S. W. (2004), Spectral evidence for zeolite in the dust on Mars, *Icarus*, *168*, 131–143, doi:10.1016/j.icarus.2003.11.003.

Ruff, S. W., and P. R. Christensen (2007), Basaltic andesite, altered basalt, and a TES-based search for smectite clay minerals on Mars, *Geophys. Res. Lett.*, *34*, L10204, doi:10.1029/2007GL029602.

Salisbury, J. W. (1993), Mid-infrared spectroscopy: Laboratory data, in *Remote Geochemical Analysis: Elemental and Mineralogical Composition*, edited by C. M. Pieters and P. A. J. Englert, pp. 79–98, Cambridge Univ. Press, New York.

Sanchez-Soto, P. J., I. Sobrados, J. Sanz, and J. L. Perez-Rodriguez (1993), ^{29}Si and ^{27}Al magic-angle-spinning nuclear magnetic resonance study of the thermal transformations of pyrophyllite, *J. Am. Ceram. Soc.*, *76*, 3024–3028, doi:10.1111/j.1151-2916.1993.tb06604.x.

Sanz, J., A. Madani, J. M. Serratosa, J. S. Moya, and S. Aza (1988), ^{27}Al and ^{29}Si magic-angle spinning nuclear magnetic resonance study of the kaolinite-mullite transformation, *J. Am. Ceram. Soc.*, *71*, C418–C421, doi:10.1111/j.1151-2916.1988.tb07513.x.

Sarikaya, Y., M. Onal, B. Baran, and T. Alemdaroglu (2000), The effect of thermal treatment on some of the physiochemical properties of a bentonite, *Clays Clay Miner.*, *48*, 557–562, doi:10.1346/CCMN.2000.0480508.

Slade, R. C. T., and T. W. Davies (1991), Evolution of structural changes during flash calcination of kaolinite: A ^{29}Si and ^{27}Al nuclear magnetic resonance spectroscopy study, *J. Mater. Chem.*, *1*, 361–364, doi:10.1039/jm9910100361.

Tomioka, N., K. Tomeoka, K. Nakamura-Messenger, and T. Sekine (2007), Heating effects of the matrix of experimentally shocked Murchison CM chondrite: Comparison with micrometeorites, *Met. Planet. Sci.*, *42*, 19–30, doi:10.1111/j.1945-5100.2007.tb00214.x.

Tonui, E. K., M. E. Zolensky, M. E. Lipschutz, M. S. Wang, and T. Nakamura (2003), Yamato 86029: Aqueously altered and thermally metamorphosed Cl-like chondrite with unusual textures, *Met. Planet. Sci.*, *38*, 269–292, doi:10.1111/j.1945-5100.2003.tb00264.x.

Tyburczy, J. A., and T. J. Ahrens (1988), Dehydration kinetics of shocked serpentine, *Proc. Lunar Planet. Sci. Conf.*, *18th*, 435–441.

Van der Marel, H. W., and H. Beutelspacher (1976), *Atlas of Infrared Spectroscopy of Clay Minerals and Their Admixtures*, 191 pp., Elsevier, Amsterdam.

Van Olphen, H., and J. J. Fripiat (1979), *Data Handbook for Clay Materials and Other Non-Metalic Minerals*, Pergamon, Oxford, U. K.

Villieras, F., J. Yvon, J. M. Cases, P. De Donato, F. Lhote, and R. Baeza (1994), Development of microporosity in clinochlore upon heating, *Clays Clay Miner.*, *42*(6), 679–688, doi:10.1346/CCMN.1994.0420604.

Wyatt, M. B., and H. Y. McSween Jr. (2002), Spectral evidence for weathered basalt as an alternative to andesite in the northern lowlands of Mars, *Nature*, *417*, 263–266, doi:10.1038/417263a.

D. L. Bish, Department of Geological Sciences, Indiana University, 1001 E. 10th St., Bloomington, IN 47405, USA.

C. Che, T. D. Glotch, and W. Xu, Department of Geosciences, State University of New York at Stony Brook, Stony Brook, NY 11794-2100, USA. (cche@ic.sunysb.edu)

J. R. Michalski, Planetary Science Institute, 1700 E. Fort Lowell, Ste. 106, Tucson, AZ 85719, USA.